Science of the Total Environment 865 (2023) 161092

Contents lists available at ScienceDirect

Science of the Total Environment

journal homepage: www.elsevier.com/locate/scitotenv

Sources, chemical components, and toxicological responses of size segregated urban air PM samples in high air pollution season in Guangzhou, China

Mo Yang [a,b,1], Hui-Xian Zeng [b,1], Xin-Feng Wang [c], Henri Hakkarainen [a], Ari Leskinen [d,e], Mika Komppula [d], Marjut Roponen [a], Qi-Zhen Wu [b], Shu-Li Xu [b], Li-Zi Lin [b], Ru-Qing Liu [b], Li-Wen Hu [b], Bo-Yi Yang [b], Xiao-Wen Zeng [b], Guang-Hui Dong [b,*], Pasi Jalava [a]

[a] Department of Environmental and Biological Science, University of Eastern Finland, Yliopistonranta 1, P.O. Box 1627, FI-70211 Kuopio, Finland
[b] Guangdong Provincial Engineering Technology Research Center of Environmental Pollution and Health Risk Assessment, Department of Occupational and Environmental Health, School of Public Health, Sun Yat-sen University, Guangzhou 510080, China
[c] Environment Research Institute, Shandong University, Qingdao 266237, China
[d] Finnish Meteorological Institute, Yliopistonranta 1, P.O. Box 1627, FI-70211 Kuopio, Finland
[e] Department of Applied Physics, University of Eastern Finland, Yliopistonranta 1, P.O. Box 1627, FI-70211 Kuopio, Finland

HIGHLIGHTS

- Emission sources highly influence the chemical components of different-sized PM.
- The inflammatory damage caused by coarse PM cannot be ignored.
- Moderate/strong correlations between PM components and toxicological effects.

GRAPHICAL ABSTRACT

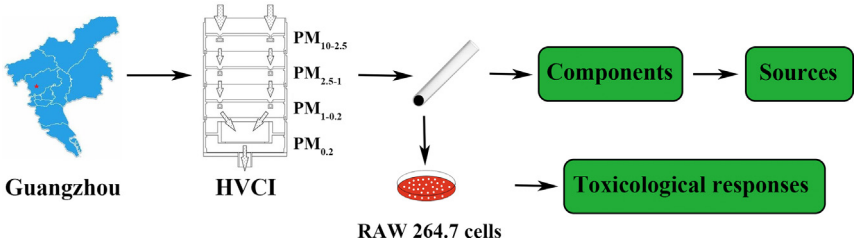

ARTICLE INFO

Editor: Jianmin Chen

Keywords:
Urban air PM
Sources
Chemical components
Toxicological responses

ABSTRACT

The sources, sizes, components, and toxicological responses of particulate matter (PM) have demonstrated remarkable spatiotemporal variability. However, associations between components, sources, and toxicological effects in different-sized PM remain unclear. The purposes of this study were to 1) determine the sources of PM chemical components, 2) investigate the associations between components and toxicology of PM from Guangzhou high air pollution season. We collected size-segregated PM samples ($PM_{10–2.5}$, $PM_{2.5–1}$, $PM_{1–0.2}$, $PM_{0.2}$) from December 2017 to March 2018 in Guangzhou. PM sources and components were analyzed. RAW264.7 mouse macrophages were treated with PM samples for 24 h followed by measurements of toxicological responses. The concentrations of $PM_{10–2.5}$ and $PM_{1–0.2}$ were relatively high in all samples. Water-soluble ions and PAHs were more abundant in smaller-diameter PM, while metallic elements were more enriched in larger-diameter PM. Traffic exhaust, soil dust, and biomass burning/petrochemical were the most important sources of PAHs, metals and ions, respectively. The main contributions to PM were soil dust, coal combustion, and biomass burning/petrochemical. Exposure to $PM_{10–2.5}$ induced the most significant reduction of cell mitochondrial activity, oxidative stress and inflammatory response, whereas DNA damage, an increase of Sub G1/G0 population, and impaired cell membrane integrity were most evident with $PM_{1–0.2}$ exposure. There were moderate or strong correlations between most single chemicals and almost all toxicological endpoints as well as between various toxicological outcomes. Our findings highlight those various size-segregated PM-induced toxicological effects in cells, and identify chemical components and sources of PM that play the key role in adverse intracellular responses. Although fine and ultrafine PM have attracted much attention, the inflammatory damage caused by coarse PM cannot be ignored.

* Corresponding author at: Guangdong Provincial Engineering Technology Research Center of Environmental Pollution and Health Risk Assessment, Department of Occupational and Environmental Health, School of Public Health, Sun Yat-sen University, 74 Zhongshan 2nd Road, Yuexiu District, Guangzhou 510080, China.
E-mail address: donggh5@mail.sysu.edu.cn (G.-H. Dong).
[1] Mo Yang and Hui-Xian Zeng contributed equally to this work.

http://dx.doi.org/10.1016/j.scitotenv.2022.161092
Received 28 September 2022; Received in revised form 16 December 2022; Accepted 17 December 2022
Available online 29 December 2022
0048-9697/© 2022 Elsevier B.V. All rights reserved.

1. Introduction

Urban air pollution, specifically particulate matter (PM), is considered among the top 5 risk factors for impaired human health and the major environmental risk factor for respiratory and cardiovascular diseases in recent decades in China (Zhou et al., 2019). Atmospheric PM is a complex mixture composed of different chemical and bacterial components from various sources, including polycyclic aromatic hydrocarbons (PAHs), ions, transition and heavy metals, and biological constituents (Rönkkö et al., 2021). A large body of research demonstrates that PM composition and toxicity can vary with particle size, source, time, and location (Jalava et al., 2015b; Lee et al., 2019; Longhin et al., 2020; Velali et al., 2018). Therefore, quantifying the contribution of specific components is key to unraveling the geographic differences in particle toxicity (Lee et al., 2019). However, studies that evaluate specific compnents of PM and their associated toxicological effects often provide conflicting results (Verma and Salana, 2022). Large-scale studies are still necessary to understand the relationships between different endpoints and PM composition.

At present, there have been many analyses of the source, composition, and toxicity of coarse PM_{10} (PM with an aerodynamic diameter < 10 μm) and $PM_{2.5}$ (PM with an aerodynamic diameter < 2.5 μm) (Lee et al., 2019). Interestingly, a previous study revealed that $PM_{0.5}$ (PM with an aerodynamic diameter < 0.5 μm) may be responsible for cardiopulmonary disease mortality upon PM exposure, and that high mortality was strongly associated with decreasing particle size (Meng et al., 2013). However, studies on the source and composition of smaller particles, and their associations with toxicological endpoints, are still limited. In particular, toxicological evidence confirms that different particle sizes can generate various toxicity (Hakkarainen et al., 2022; Rönkkö et al., 2021; Rönkkö et al., 2018a), However, the present air quality guidelines suppose that all PM is equally toxic, and the causal relationship between toxicological responses and components of different-sized PM remains undefined. Thus, multidisciplinary studies to investigate specific PM components and their interactions with toxicological endpoints in different particle sizes derived from diverse emission sources are needed.

Provincial capitals in China, with developed economies and industries, dense populations, and congested traffic, are the most seriously affected by PM pollution (Chen and Xu, 2017). Guangzhou is recognized as the most economically developed and densely populated first-tier city in China along with Beijing, Shanghai and Shenzhen, and is the capital city of Guangdong Province. PM concentration in Guangzhou peaks from December to March of the following year, and is affected by the winter heating in northern China, sources of industry, biomass combustion and vehicle exhaust etc., and climate (Fan et al., 2015). Although the average annual PM concentration in Guangzhou is considered relatively low in China, the risk of cardiopulmonary diseases attributed to PM in Guangzhou is very high in China (Bhatia-Barnes et al., 2017; Li et al., 2021). Therefore, the toxicological effects PM concentration during the high pollution season in Guangzhou cannot be ignored due to its strong adverse impact on human.

Combining emission sources, compositions, and toxicological endpoints of four size-segregated PM samples would offer a comprehensive understanding of how chemical components and emission sources affect the toxicological characteristics of PM. As such, this study aimed to determine the main emission sources for PM and how this affects its composition. Furthermore, associations between specific PM components and toxicological endpoints of four size-segregated PM samples ($PM_{10–2.5}$, $PM_{2.5–1}$, $PM_{1–0.2}$, and $PM_{0.2}$, where $PM_{0.2}$ with aerodynamic diameter ≤ 0.2 μm, and $PM_{10–2.5}$, $PM_{2.5–1}$ and $PM_{1–0.2}$ denotes PM with aerodynamic diameter range from 10-2.5 μm, 2.5–1 μm, and 1–0.2 μm, respectively) during high air pollution season in Guangzhou were investigated. We collected the PM samples from December 2017 to March 2018 in Guangzhou. Combining various compositions, emission sources and toxicological endpoints of four size-segregated PM samples would offer a comprehensive understanding of how chemical components and emission sources affect the toxicological characteristics of PM.

2. Materials and methods

2.1. PM sampling, collection, and extraction

The size-segregated PM samples ($PM_{10–2.5}$, $PM_{2.5–1}$, $PM_{1–0.2}$, $PM_{0.2}$) were collected on the ten-story building roof (without any nearby higher buildings) at the Sun Yat-sen University North campus with a high-volume cascade impactor (HVCI) from December 2017 to March 2018. Sampling parameters, flow rates, and sampling filters for HVCI, and the process for PM extraction, have been detailed in our previous studies (Jalava et al., 2006; Jalava et al., 2015b). Briefly, after weighing, the sampling filter was first washed with methanol, then concentrated by a rotary evaporator, and finally dried with nitrogen to obtain the particles. Detailed sampling information is provided in Supplementary material Table S4. All the PM samples were stored at −20 °C for chemical component analysis and toxicology experiments.

2.2. PM concentration monitoring

The continuous mass concentrations of $PM_{2.5}$, PM_1 and $PM_{0.2}$ were monitored in the same location as PM collection by using a Nanoscan SMPS (scanning mobility particle sizer Model 3910, TSI incorporated, USA) and an Optical Particle Sizer Spectrometer (Model 3330, TSI incorporated, USA). Temperature and relative humidity were also monitored, with a weather transmitter (WXT 520, VAISALA, Finland). The concentrations of $PM_{10–2.5}$, $PM_{2.5–1}$, $PM_{1–0.2}$ and $PM_{0.2}$ were calculated based on the HVCI sampled mass and flow.

2.3. PM chemical components analysis

The concentrations of ions [sodium (Na^+), ammonium (NH_4^+), potassium (K^+), lithium (Li^+), magnesium (Mg^{2+}), calcium (Ca^{2+}), fluoride (F^-), chloride (Cl^-), bromine (Br^-), nitrite (NO_2^-), nitrate (NO_3^-), sulfate (SO_4^{2-}), phosphate (PO_4^{3-})] in the PM samples were analyzed by ion chromatography (Dionex ICS-1100, Thermo Fisher, USA). PM samples were washed with ultrapure water and filtered into different tubes. The chromatographic separation column used for anions was Ionpac AS19 (4*250 mm) chromatographic column, and an Ionpac CS12A (4*250 mm) chromatographic column was used for cations. The detection limits are shown in Supplementary materials Table S1.

The concentrations of metallic elements [beryllium (Be), sodium (Na), magnesium (Mg), aluminum (Al), silicon (Si), potassium (K), calcium (Ca), vanadium (V), chromium (Cr), manganese (Mn), iron (Fe), Cobalt (Co), nickel (Ni), copper (Cu), zinc (Zn), arsenic (As), selenium (Se), strontium (Sr), yttrium (Y), cadmium (Cd), stannum (Sn), antimony (Sb), barium (Ba), cerium (Ce), thallium (Tl), lead (Pb), uranium (U)] in PM samples were analyzed by inductively coupled plasma mass spectrometer (ICP-MS, Thermo Fisher-iCAP RQ, USA). PM samples were eluted and nitrified with an acid mixture (5.55 % nitric acid HNO_3 + 16.55 % hydrochloric acid HCl + 77.9 % ultrapure water). After nitrification, samples were filtered into different tubes and fixed to the same volume with ultrapure water, and finally detected via ICP-MS. The detection limits are shown in Supplementary materials Table S2.

The concentrations of 18 PAHs [Naphthalene (NA), Acenaphthene (AC), Acenaphthylene (ACL), Fluorene (FL), Phenanthrene (PHE), Anthracene (AN), Fluoranthene (FA), Pyrene (PY), Benzo(*a*)anthracene [B(*a*)A], Chrysene (CHR), Benzo(*b*)fluoranthene [B(*b*)FA], Benzo(*k*)fluoranthene [B(*k*)FA], Benzo(*j*)fluoranthene [B(*j*)FA], Benzo(*e*)pyrene [B(*e*)P], Benzo(*a*)pyrene [B(*a*)P], Indeno(1,2,3-*cd*)pyrene (IP), Dibenzo(*a*,*h*)anthracene [DB(*a*,*h*)A], Benzo(*g*,*h*,*i*)perylene [B(*g*,*h*,*i*)P]] in the PM samples were analyzed by gas chromatography tandem mass spectrometer (Agilent GC–MS 7890B-5977A, USA). An Agilent HP-5MS (30 m*0.25 mm*0.25 μm) column was used for the separation of the compounds. The instrument was operated in the selected ion monitoring (SIM) mode. The PM samples were washed with the mixture (dichloromethane: methanol = 97:3) and dried with nitrogen repeatedly. Then, the 0.5 mL concentrate after nitrogen

was washed five times in the activated anhydrous sodium sulfate chromatography column with the eluent (dichloromethane: n-hexane = 1:1). The15 mL sample solution was dried with nitrogen to 1–2 mL, and washed in the activated silica gel purification chromatography column. The washing and drying steps were repeated. Finally, the dried PM sample was dissolved in 300 μL n-hexane and detected on the GC–MS. The detection limits and the recovery rate of PAHs are shown in Supplementary materials Table S3 and Table S5.

2.4. Source appointment by positive matrix factorization model

A positive matrix factorization (PMF) receptor model (USEPA, PMF 5.0) was used to identify the major sources of particulate components in different size ranges and to quantify the relative contributions from different sources. Two files are needed as the PMF model inputs: the concentration and the uncertainty data. These values were determined using the equations below (Arruti et al., 2011; Polissar et al., 1998):

For the concentration values lower than the detection limits:

$$x_{ij} = \frac{DL_i}{2}, \sigma_{ij} = \frac{5DL_i}{6} \quad (1)$$

For the concentration values higher than the detection limits:

$$x_{ij} = c_{ij} \quad (2)$$

$$\text{If } x_{ij} \le 3DL_i, \sigma_{ij} = \frac{DL_i}{3} + 0.2 \times c_{ij} \quad (3)$$

$$\text{If } x_{ij} > 3DL_i, \sigma_{ij} = \frac{DL_i}{3} + 0.1 \times c_{ij} \quad (4)$$

where x_{ij} is the concentration value of the species *i* for the sample *j*, DL_i is the detection limit of the species *i*, σ_{ij} is the uncertainty value corresponding to the concentration x_{ij}, and c_{ij} is the measured concentration. Note that the sample data with missing values were not included in the input data file. The predicted concentrations and the observed concentrations of PM and major components were substantially consistent (Yang et al., 2022b). The PMF model was run 40 times and the optimal result was chosen as outputs based on the minimum bootstrap error. The basic outputs of the PMF model included factor profiles and the uncertainties, factor contributions for each sample, and the residuals of the prediction values when comparing with the observation values. The bootstrap error estimation was determined by minimum Q/Qexp value (Li et al., 2020; Zhang et al., 2018).

In this study, a total of 41 variables were selected as the input of the PMF model, including the mass concentration of PM (i.e. $PM_{10-2.5}$, $PM_{2.5-1}$, $PM_{1-0.2}$, or $PM_{0.2}$), seven major water-soluble ions of sulfate, nitrate, chloride, ammonium, sodium, potassium, and calcium, fifteen trace elements of Si, Al, Fe, Ba, Sr, Mn, Cr, Ni, Cu, Zn, As, Cd, Ph, Sn, and Sb, and eighteen PAHs of NA, ACL, AC, FL, AN, PHE, FA, FY, BaA, CHR, BbFA, BkFA, BjFA, BeP, BaP, IO, DBahA, and BghiP. There were 128 samples (i.e. 128 data sets) in total to run the PMF model. Factors were recognized and interpreted primarily according to two a priori criteria: investigation of the retrieved factor profiles for distinct chemical signatures and comparison of the time series of the factors with tracers. To obtain optimal source apportionment results, three to eight factors were tested and evaluated separately. The selection for the proper number of factors was based on an integrated analysis of the Q/Qexp value, scaled residuals, the residual time series as a function of the number of factors, the variability of each variable attributed to the sources was examined from the bootstrap approach and was within the acceptable range, and the reasonableness of the resolved factors as individual sources. Finally, a five-factor solution was selected. Note that solutions with less than five factors showed obvious increase in scaled residuals and a combination of metal smelting, biomass burning, and coal combustion related factors, while solutions with more than five factors presented a split of biomass burning and the traffic factors (Yang et al., 2022b).

2.5. Cell culture

RAW264.7 (a mouse macrophage cell line) were obtained from American Type Culture Collection (ATCC). RAW264.7 cells were cultured in RPMI 1640 cell culture medium (Life Technologies) supplemented with 10 % heat-inactivated fetal bovine serum (FBS) (Sigma, USA), 1 % L-Glutamine and 1 % Penicillin-streptomycin (Life Technologies, USA) in a 5 % CO_2 atmosphere at 37 °C. In the experiments, the cell suspension was diluted to 1.5×10^5 cells/mL and cultured on 24-well plate (Costar, Corning, NY, USA) for 24 h to allow the cells to adhere and divide. In the MTT test experiment, the cell suspension was diluted to 5×10^4 cells/mL and cultured on 96-well plate. Fresh medium was changed and RAW264.7 cells were allowed to stabilize for one hour before the PM exposure experiment.

2.6. PM exposure

Tubes containing the PM sample were put in ultrasonic bath for 30 min to suspend the PM samples into pyrogen free water (Sigma W1503, USA) and dimethyl sulfoxide (DMSO) at the concentration of 5 mg/mL before the exposure experiment. The cells were treated with control (pyrogen free water) and four doses (12.5, 50, 100 and 200 μg/mL) of PM samples for 24 h. All experiments were carried out with at least three replicates. After PM exposure for 24 h, the culture medium was collected and stored at −80 °C, and the RAW264.7 cells were scratched off from the bottom of each well using the cell scratcher with 600 μL cold phosphate buffered saline (PBS). We centrifuged all the cell tubes (8000 rpm, 5 min, 4 °C) to obtain cells and resuspended RAW264.7 cells with 500 μL cold PBS for the toxicological analyses.

2.7. Toxicological analysis

2.7.1. MTT test

Mitochondrial activity of RAW264.7 cells was tested with the MTT assay. MTT-solution (25 μL) was added to each well, and incubated 2 h at 37 °C after PM exposure, then sodium dodecyl sulfate (SDS) buffer (100 μL) was added to each well, and incubated overnight at 37 °C. The absorbance of the RAW264.7 cells was tested with the spectrophotometric plate reader (BioTek, SYNERGY H1, USA). The viability of the RAW264.7 cells was calculated as multiples of the control group. Potential affection of PM samples itself with the MTT assay was tested and ruled out.

2.7.2. Cell membrane integrity and DCF

Cell membrane integrity of RAW 264.7 cells was detected with propidium iodide (PI) exclusion assay. Intracellular oxidative stress of RAW264.7 cells was detected with 2′,7′- dichlorofluorescein (DCF) assay. 100 μL RAW264.7 cells (each sample has a duplicate well) was placed in a 96-well plate, and DCF solution (8 μL) was added to each well. The absorbance was immediately detected with the spectrophotometric plate reader (BioTek, SYNERGY H1, USA), and detected every 30 min after incubation at 37 °C twice. Then, PI solution (7.2 μL) was added to each well, and the plate was stirred briefly and incubated 20 min at 37 °C. Absorbance was tested by the reader. Following reading, 10 % Triton X-100 (20 μL) was added to each well, and the plate was stirred on a plate shaker and incubated 20 min at room temperature. Finally, we measured the absorbance again once.

2.7.3. Cell cycle

200 μL RAW264.7 cells was fixed to cold 70 % ethanol (4 mL). RAW264.7 cells were centrifuged (480 *g*, 5 min, 4 °C), and all the ethanol was removed. The cells were washed once with cold PBS (1 mL) and resuspended in cold PBS (250 μL). RNAse A (10 mg/mL, 7.5 μL) was added to each sample tube, the cell was vortexed and incubated 1 h at 50 °C. Then, PI solution (4 μL) was added, the cell was vortexed and incubated 30 min at 37 °C. Cell cycle phases were analyzed by flow cytometric analysis with BD FACSCanto™ II (BD Biosciences, San Jose, CA USA).

2.7.4. Comet assay

60 μL RAW264.7 cells (each sample has a duplicate tube) was placed in 540 μL freeze medium (40 % filtrated FBS, 50 % RPMI, 10 % DMSO) and frozen at −80 °C until detected. RAW264.7 cells were thawed and centrifuged (8000 rpm, 5 min, 4 °C). 50 μL medium was left in the tube, and cell suspension (20 μL) was mixed with 0.5 % low melting point agarose (LMPA) (80 μL). The cell LMPA mixture (80 μL) was placed on a microscope slide which was covered with 1 % normal melting point agarose (NMPA). A glass cover plate was added on the microscope slide and removed after 5 min. The cold lysis buffer was added onto the microscope slides for 1 h at 4 °C, and then all the microscope slides were put in the electrophoresis chamber. Electrophoresis buffer was added to the electrophoresis chamber and incubated for 40 min, avoiding light. After that, the microscope slides started to be electrophoresed for 20 min at 24 V/300 mA, and were removed and rinsed 3 times with neutralization buffer. 99 % ethanol was fixed to the DNA on the microscope slides for 10 min. Then, the microscope slides were dried at room temperature overnight and stored in dark conditions. Diluted ethidium bromide dye (75 μL) was pipetted onto the microscope slides, and glass cover plate was used to cover microscope slide for at least 30 min. The nuclei in ethidium bromide (100 cells per dose) were analyzed by the special image analysis system (Comet assay IV, Perceptive Instruments Ltd., Suffolk, UK). Tail intensity was used as the parameter in the statistical analysis.

2.7.5. Inflammatory mediators

Tumor necrosis factor alpha (TNF-α) and macrophage inflammatory protein 2 (MIP-2) were immunochemically analyzed by commercial enzyme linked immunosorbent assay (ELISA) kits (R&D Systems, Minneapolis, MN, USA) from cell culture medium according to the manufacturers' recommendations. Absorbance was detected with the spectrophotometric plate reader (BioTek, SYNERGY H1, USA). The mouse TNF-α and MIP-2 ELISA kits were DuoSet ELISA. The assay range for TNF-α and MIP-2 concentrations were 31.2–2000 pg/mL and 15.6–1000 pg/mL, respectively.

2.8. Statistical analysis

All the experiment results of different doses were compared using one-way ANOVA, followed by the LSD method for the comparison between the two groups. Non-parametric Spearman correlation was used to examine the associations between different toxicological endpoints, and the associations between toxicological endpoints and PM components. p-value <0.05 was considered to be statistically significant.

3. Results

3.1. PM concentration and meteorological parameters

The calculated average concentrations of size-segregated particulate samples from December 2017 to March 2018 in Guangzhou are shown in Fig. 1A. The mean concentrations of $PM_{10–2.5}$, $PM_{2.5–1}$, $PM_{1–0.2}$ and $PM_{0.2}$ were 39.77, 25.32, 37.90 and 6.34 μg/m^3, respectively. Table 1 presents the continuous air PM concentration, temperature and relative humidity from December 2017 to March 2018, in Guangzhou. The mean concentrations of $PM_{2.5}$, PM_1 and $PM_{0.2}$ were 70.72, 67.00 and 8.75 μg/m^3, respectively. Mean temperature and relative humidity were 18.33 °C and 56.25 %.

3.2. PM chemical components and sources

Fig. 1B-D illustrates the mass concentration of water-soluble ions, metallic elements, and PAHs in particulate samples from December 2017 to March 2018 in Guangzhou. The total contents of ions and PAHs in the size-segregated particulate samples were $PM_{0.2} > PM_{1–0.2} > PM_{2.5–1} > PM_{10–2.5}$. The opposite was observed for metallic elements in the PM samples, i.e. $PM_{10–2.5} > PM_{2.5–1} > PM_{1–0.2} > PM_{0.2}$. Coal combustion, metal smelting, traffic exhaust, biomass burning, and soil dust were recognized as the five major sources of PM and particulate components, based on the PMF model results. Detailed information on the identification and interpretation of each source can be seen in our previous study (Yang et al., 2022b). Note that the variability in the contribution of each factor to the individual sources is generally fell in the acceptable limits (Yang et al., 2022b).

Fig. 2 shows the sources of particulate components in Guangzhou from December 2017 to March 2018. Soil dust was the source that contributed the most to $PM_{10–2.5}$, but contributed the least to $PM_{0.2}$; coal combustion was the source that contributed the most to $PM_{2.5–1}$ and $PM_{1–0.2}$, while metal smelting was the source that contributed the least to them; biomass burning/petrochemical was the source that contributed the most to $PM_{0.2}$ (Fig. 2A). As shown in Fig. 2B, overall, soil dust and coal combustion were the major sources of total PM. Coal combustion was the main source of sulfate, ammonium, potassium, chloride, and nitrate. Soil dust and biomass burning/petrochemical were also the main sources of nitrate, sodium, and calcium. Soil dust served as the most prominent source of Si, AL, Fe, Ba, Sr, Mn, Cr and Ni; while metal smelting was a major contributing source of Cu, Zn, As, Cd, Pb, Sn, and Sb. Biomass burning/petrochemical was the primary source of some PAHs (ACL, NA, AC, FL, and AN), contributing >30 %; while traffic exhaust was the major source of other PAHs [B(*g*,*h*,*i*)P, B(*a*)P, IP, B(*k*)FA, B(*j*)FA, B(*e*)P, B(*a*)A, B(*b*)FA, DB(*a*,*h*)A, CHR, PY]. Detailed data is shown in supplementary materials Table S6.

3.3. Toxicological endpoints

Fig. 3 shows the mitochondrial activity, intracellular oxidative potential, cell cycle Sub G1/G0 phase, genotoxicity and inflammatory mediators (TNF-α and MIP-2) of RAW264.7 macrophages after exposure to size-segregated particulate samples in Guangzhou from December 2017 to March 2018. All PM samples induced dose-dependent decreases of MTT in the four size-segregated particulate samples, especially in $PM_{10–2.5}$ (Fig. 3A). All PM samples induced significant increases in DCF (Fig. 3B), with the greatest increase observed for $PM_{10–2.5}$. The four size-segregated particulate samples induced dose-dependent increases of cell cycle Sub-G1/G0 population; exposure to $PM_{10–2.5}$ caused small changes, while large changes were observed with exposure to $PM_{1–0.2}$ and $PM_{0.2}$ (Fig. 3C). All PM samples caused significant increases of DNA tail intensity, especially in $PM_{1–0.2}$ (Fig. 3D). Genotoxicity of $PM_{10–2.5}$, $PM_{2.5–1}$ and $PM_{0.2}$ were similar (Fig. 3D). The four size-segregated particulate samples all induced dose-dependent increases of TNF-α and MIP-2, with the largest increases observed with exposure to $PM_{10–2.5}$ (Fig. 3E, F).

3.4. Associations of PM components with toxicological endpoints

Table 2 shows the associations of PM inorganic components with cytotoxic responses, oxidative damage and inflammation with the four size-segregated particulate samples in the 100 μg/mL group cells. A stronger association with inflammatory mediators, especially MIP-2, was observed with ions and metals in all PM samples. Cr, Ni, Zn, Sn and Ba were positively associated with MTT, and negatively associated with DCF in $PM_{10–2.5}$. Ions and metal elements have the strongest correlation with MTT in $PM_{0.2}$. DCF was most affected by ions and metal elements in $PM_{2.5–1}$. Table 3 shows the associations of PM organic components PAHs with cytotoxic responses, oxidative damage and inflammation in the 100 μg/mL group cells of the four size-segregated particulate samples. The largest number of associations was observed between PAHs and MTT in $PM_{10–2.5}$ and $PM_{2.5–1}$. PAHs and DCF negatively associated in most PM samples. PAHs were strongly associated with inflammatory mediators in most PM samples. Table 4 shows the associations of PM inorganic components with DNA replication and damage in the 100 μg/mL group cells of the four size-segregated particulate samples. DNA tail intensity was affected by ions and metal elements in most PM samples. Some ions and metal elements were strongly ($\rho = 0.95$ or -0.95) associated with cell cycle Sub G1/G0 phase. Table 5 shows the associations of PM organic components PAHs with DNA replication and damage in the 100 μg/mL group cells.

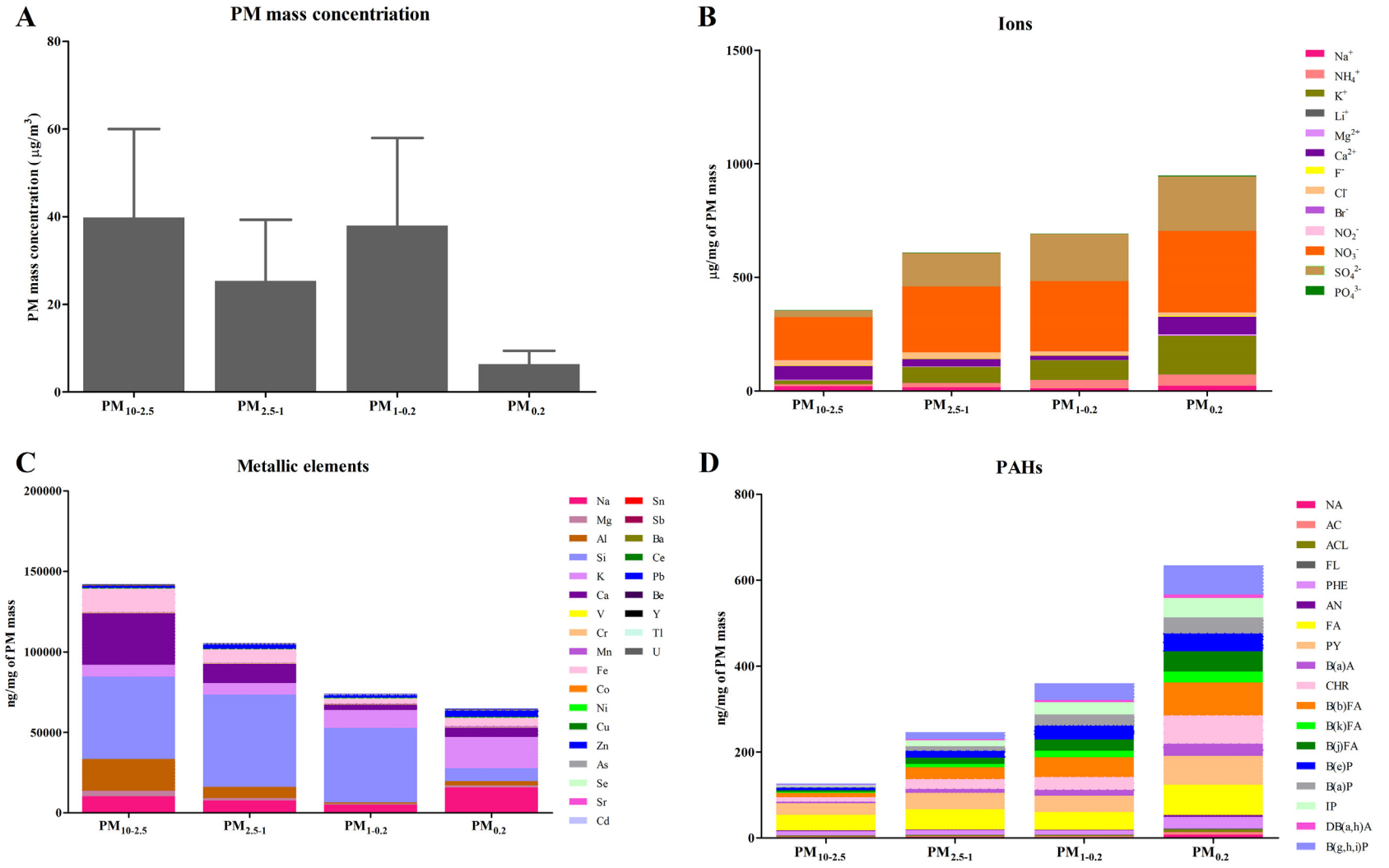

Fig. 1. Calculated average concentrations of size-segregated particulate samples and mass concentration of water-soluble ions, metallic elements, PAHs in particulate samples from December 2017 to March 2018 in Guangzhou. A: Calculated average concentrations of size-segregated particulate samples; B-D: concentrations of ions, metallic elements and PAHs in size-segregated particulate samples.

Table 1
Continuous air PM concentration measurements, temperature and relative humidity from December 2017 to March 2018, in Guangzhou.

	Mean	SD	Median	25th	75th
Mass concentration (μg/m^3)					
$PM_{2.5}$	70.72	49.18	61.73	36.37	92.17
PM_1	67.00	47.03	58.26	34.07	87.44
$PM_{0.2}$	8.75	5.10	7.97	4.97	11.02
Temperature (°C)	18.33	5.08	19.20	15.40	22.00
Relative Humidity (%)	56.25	15.98	58.60	44.50	67.50
Wind speed (m/s)	1.48	1.14	1.10	0.70	2.00
Wind direction (degrees)	180.38	123.93	178.00	60.00	316.00

More than half of the 18 PAHs were significantly associated with DNA tail intensity in $PM_{10–2.5}$, $PM_{2.5–1}$ and $PM_{1–0.2}$.

Fig. 4 shows the associations of PM components (total ions, metals, PAHs) with toxicological endpoints in size-segregated particulate samples. There was a negative trend between MTT and ions, metallic elements, PAHs across the four particle sizes. In most conditions, a positive correlation was observed between DCF, cell cycle (Sub G1/G0 phase), DNA tail intensity, inflammatory factor (TNF-α, MIP-2) and ions, metallic elements, PAHs. Fig. S1 shows the PI viability of RAW264.7 macrophages after exposure to size-segregated PM and the associations of PM components (total ions, metals, PAHs) with PI viability. There were changes only in the 200 μg/mL group from $PM_{2.5–1}$, $PM_{1–0.2}$ and $PM_{0.2}$. Furthermore, a negative trend was observed between PI viability and ions, metallic elements, PAHs.

3.5. Associations of toxicological endpoints

Fig. S2–5 show the associations of different toxicological endpoints for the four size-segregated particulate samples. There were significant negative associations between MTT and all the toxicological endpoints in $PM_{10–2.5}$, $PM_{2.5–1}$ amd $PM_{0.2}$ (Fig. S2, 3, 5, A-E). Significant negative associations were also observed between MTT and cell cycle Sub G1/G0 phase, DNA tail intensity, inflammatory mediators in $PM_{1–0.2}$ (Fig. S4, A-E). DCF was significantly positively associated with DNA tail intensity and inflammatory mediators in $PM_{10–2.5}$ (Fig. S2, G-I). DCF was also

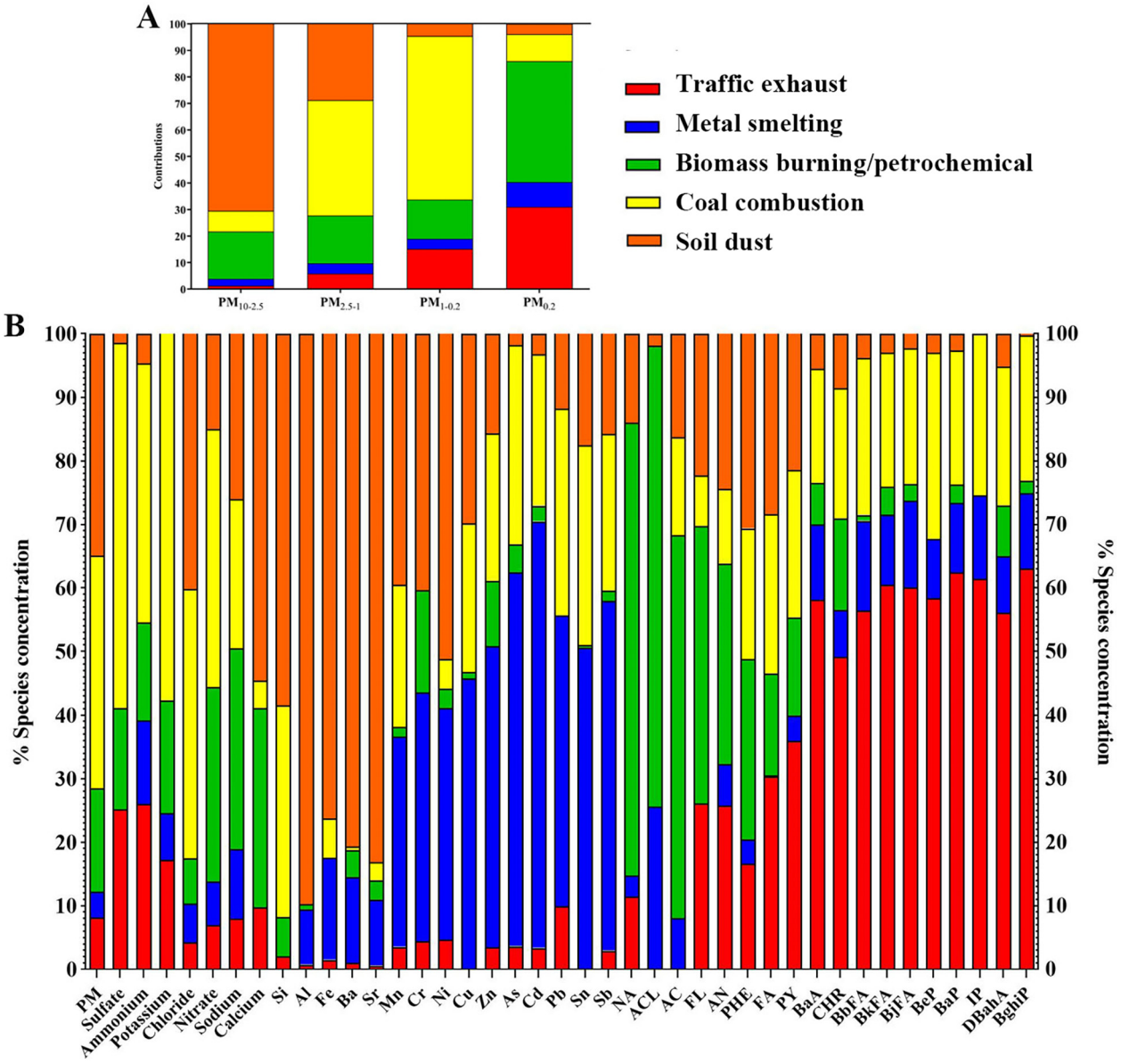

Fig. 2. Sources of particulate components in Guangzhou from December 2017 to March 2018. A: sources of size-segregated particulate samples; B: sources of PM, ions, metallic elements and PAHs in particulate samples.

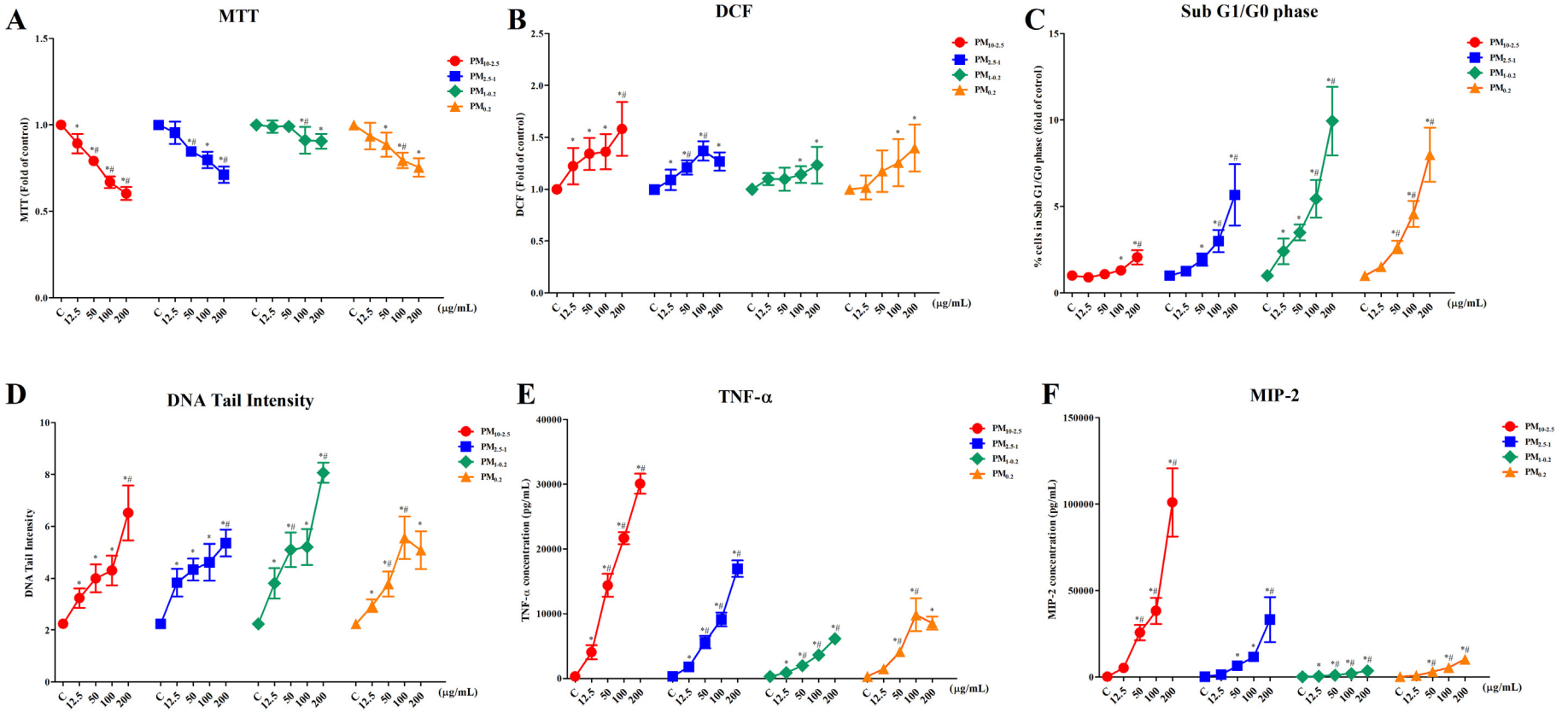

Fig. 3. Mitochondrial activity, intracellular oxidative potential, cell cycle Sub G1/G0 phase, genotoxicity and inflammatory mediators (TNF-α and MIP-2) of RAW 264.7 macrophages after exposure to four doses of size-segregated particulate samples in Guangzhou from December 2017 to March 2018. *Significant differences between the exposure group and the control group ($P < 0.05$). # Significant differences between the high dose group and the low dose group ($P < 0.05$).

Table 2
Associations of PM inorganic components with cytotoxic responses, oxidative damage and inflammatory in the 100 μg/mL group cells.

Items	$PM_{10-2.5}$				$PM_{2.5-1}$				$PM_{1-0.2}$				$PM_{0.2}$			
	MTT	DCF	TNF-α	MIP-2	MTT	DCF	TNF-α	MIP-2	MTT	DCF	TNF-α	MIP-2	MTT	DCF	TNF-α	MIP-2
Ions	0.24	−0.60	**0.54***	0.47	0.33	**0.74***	**0.56***	**0.62***	−0.33	−0.05	0.28	**0.89****	0.37	**0.79***	**−0.60***	0.21
Na^+	0.24	−0.60	**0.54***	0.47	0.33	**0.74***	**0.56***	**0.62***	−0.33	−0.05	0.28	**0.89****	**0.90****	0.63	0.48	**0.77****
NH_4^+	−0.47	0.07	0.21	**0.95****	−0.33	**−0.74***	**−0.56***	**−0.62***	−0.36	**−0.69***	**−0.92****	**−0.53***	−0.53	0.16	**−0.94****	**−0.58***
K^+	0.24	−0.60	**0.54***	0.47	0.33	**0.74***	**0.56***	**0.62***	−0.33	−0.05	0.28	**0.89****	**0.90****	**0.63**	0.48	**0.77****
Ca^{2+}	−0.24	0.60	**−0.54***	−0.47	**−0.74***	−0.05	**−0.85****	**−0.80***	−0.33	−0.05	0.28	**0.89****	**0.90****	0.63	0.48	**0.77****
Cl^-	0.24	−0.60	**0.54***	0.47	0.33	**0.74***	**0.56***	**0.62***	**0.73***	**0.74***	0.50	−0.37	**0.90****	0.63	0.48	**0.77****
NO_3^-	−0.47	0.07	0.21	**0.95****	0.33	**0.74***	**0.56***	**0.62***	**0.73***	**0.74***	0.50	−0.37	**0.90****	0.63	0.48	**0.77****
SO_4^{2-}	0.24	−0.60	**0.54***	0.47	0.33	**0.74***	**0.56***	**0.62***	−0.33	−0.05	0.28	**0.89****	0.37	**0.79***	**−0.60***	0.21
TE	0.47	−0.07	−0.21	**−0.95****	**0.74***	0.05	**0.85****	**0.80***	**0.73***	**0.74***	0.50	−0.37	0.37	**0.79***	**−0.60***	0.21
Al	0.47	−0.07	−0.21	**−0.95****	0.33	**−0.69***	0.29	0.18	0.33	0.05	−0.28	**−0.89****	0.53	−0.16	**0.94****	**0.58***
Si	0.47	−0.07	−0.21	**−0.95****	**0.74***	0.05	**0.85****	**0.80***	**0.73***	**0.74***	0.50	−0.37	−0.37	**−0.79***	**0.60***	−0.21
Cr	**0.79****	**−0.67***	0.30	−0.47	0.33	**−0.69***	0.29	0.18	**0.73***	**0.74***	0.50	−0.37	0.37	**0.79***	**−0.60***	0.21
Mn	0.47	−0.07	−0.21	**−0.95****	0.33	**−0.69***	0.29	0.18	0.33	0.05	−0.28	**−0.89****	**0.90****	**0.63**	0.48	**0.77****
Fe	0.47	−0.07	−0.21	**−0.95****	0.33	**−0.69***	0.29	0.18	**0.73***	**0.74***	0.50	−0.37	**0.90****	0.63	0.48	**0.77****
Ni	**0.79****	**−0.67***	0.30	−0.47	**0.74***	0.05	**0.85****	**0.80***	0.36	**0.69***	**0.92****	**0.53***	**0.90****	0.63	0.48	**0.77****
Cu	0.47	−0.07	−0.21	**−0.95****	0.33	**−0.69***	0.29	0.18	0.33	0.05	−0.28	**−0.89****	−0.37	**−0.79***	**0.60***	−0.21
Zn	**0.79****	**−0.67***	0.30	−0.47	0.33	**−0.69***	0.29	0.18	0.33	0.05	−0.28	**−0.89****	0.53	−0.16	**0.94****	**0.58***
As	0.47	−0.07	−0.21	**−0.95****	0.33	**−0.69***	0.29	0.18	−0.36	**−0.69***	**−0.92****	**−0.53***	**−0.90****	−0.63	−0.48	**−0.77****
Sr	0.47	−0.07	−0.21	**−0.95****	0.33	**0.74***	**0.56***	**0.62***	0.36	**0.69***	**0.92****	**0.53***	**0.90****	0.63	0.48	**0.77****
Cd	0.47	−0.07	−0.21	**−0.95****	−0.33	**−0.74***	**−0.56***	**−0.62***	−0.36	**−0.69***	**−0.92****	**−0.53***	**−0.90****	−0.63	−0.48	**−0.77****
Sn	**0.79****	**−0.67***	0.30	−0.47	0.33	**−0.69***	0.29	0.18	0.33	0.05	−0.28	**−0.89****	−0.37	**−0.79***	**0.60***	−0.21
Sb	0.47	−0.07	−0.21	**−0.95****	0.33	**−0.69***	0.29	0.18	0.33	0.05	−0.28	**−0.89****	**−0.90****	−0.63	−0.48	**−0.77****
Ba	**0.79****	**−0.67***	0.30	−0.47	0.33	**−0.69***	0.29	0.18	0.36	**0.69***	**0.92****	**0.53***	0.53	−0.16	**0.94****	**0.58***
Pb	0.47	−0.07	−0.21	**−0.95****	−0.33	**−0.74***	**−0.56***	**−0.62***	−0.36	**−0.69***	**−0.92****	**−0.53***	**−0.90****	−0.63	−0.48	**−0.77****

The values are Spearman's correlation coefficients (ρ). Asterisks indicate statistical significance * ($P < 0.05$) and ** ($P \leq 0.001$). TE: total elements.

positively associated with all the toxicological endpoints in $PM_{2.5-1}$, $PM_{1-0.2}$, and $PM_{0.2}$ (Fig. S3–5, G-I). Cell cycle Sub G1/G0 phase was significantly positively associated with DNA tail intensity and inflammatory mediators in all the PM samples (Fig. S2–5, J-L). There were significant negative associations between DNA tail intensity and inflammatory mediators in all the PM samples (Fig. S2–5, M-O).

Fig. S6–9 show the associations of PI viability (cell membrane integrity) with other toxicological endpoints across the four size-segregated particulate samples. PI viability was significantly negatively associated with cell cycle Sub G1/G0 phase in $PM_{10-2.5}$ and $PM_{2.5-1}$ (Fig. S6C, S7C). PI viability was negatively associated with inflammatory mediators in $PM_{2.5-1}$ and $PM_{1-0.2}$ (Fig. S7, 8, *E*-F). PI viability was significantly negatively associated with DNA tail intensity (Fig. S8A), and positively associated with MTT (Fig. S8D) in $PM_{1-0.2}$. PI viability was significantly negatively associated with DCF in $PM_{0.2}$ (Fig. S9B).

4. Discussion

In this study, it was discovered that $PM_{10-2.5}$ and $PM_{1-0.2}$ concentrations were relatively higher in the four size-segregated PM samples collected form Guangzhou. For the chemical components in PM, $PM_{0.2}$ contained most ions and PAHs, and $PM_{10-2.5}$ contained most metallic elements. As to the sources of PM, soli dust contributed more approximately two thirds to coarse particles, while coal combustion and biomass burning/petrochemical served as the major sources to fine particles including $PM_{2.5-1}$, $PM_{1-0.2}$, and $PM_{0.2}$. $PM_{10-2.5}$ resulted in the strongest reduction of cell mitochondrial activity, increase of intracellular oxidative potential and upregulation of inflammatory mediators, while $PM_{1-0.2}$ led to the most distinct generation of sub G1/G0 phase population, induction of DNA damage and destruction of cell membrane integrity. The majority of single chemical components measured across the four size-segregated PM

Table 3
Associations of PM organic components PAHs with cytotoxic responses, oxidative damage and inflammatory in the 100 μg/mL group cells.

Items	$PM_{10-2.5}$				$PM_{2.5-1}$				$PM_{1-0.2}$				$PM_{0.2}$			
	MTT	DCF	TNF-α	MIP-2	MTT	DCF	TNF-α	MIP-2	MTT	DCF	TNF-α	MIP-2	MTT	DCF	TNF-α	MIP-2
PAHs	**0.79****	**−0.67***	0.30	−0.47	0.33	**−0.69***	0.29	0.18	−0.36	**−0.69***	**−0.92****	**−0.53***	−0.37	**−0.79***	**0.60***	−0.21
NA	−0.47	−0.07	0.21	**0.95****	**0.74***	0.05	**0.85****	**0.80***	−0.33	−0.05	0.28	**0.89****	**0.90****	0.63	0.48	**0.77****
AC	0.24	−0.60	**0.54***	0.47	0.33	**−0.69***	0.29	0.18	−0.33	−0.05	0.28	**0.89****	0.53	−0.16	**0.94****	**0.58***
ACL	0.47	−0.07	−0.21	**−0.95****	**0.74***	0.05	**0.85****	**0.80***	0.36	**0.69***	**0.92****	**0.53***	**0.90****	0.63	0.48	**0.77****
FL	0.24	−0.60	**0.54***	0.47	0.33	**−0.69***	0.29	0.18	−0.33	−0.05	0.28	**0.89****	0.37	**0.79***	**−0.60***	0.21
PHE	0.24	−0.60	**0.54***	0.47	**0.74***	0.05	**0.85****	**0.80***	−0.36	**−0.69***	**−0.92****	**−0.53***	−0.37	**−0.79***	**0.60***	−0.21
AN	**0.79****	**−0.67***	0.30	−0.47	**0.74***	0.05	**0.85****	**0.80***	**−0.73***	**−0.74***	−0.50	0.37	**0.90****	0.63	0.48	**0.77****
FA	**0.79****	**−0.67***	0.30	−0.47	**0.74***	0.05	**0.85****	**0.80***	0.33	0.05	−0.28	**−0.89****	−0.37	**−0.79***	**0.60***	−0.21
PY	**0.79****	**−0.67***	0.30	−0.47	**0.74***	0.05	**0.85****	**0.80***	0.33	0.05	−0.28	**−0.89****	−0.37	**−0.79***	**0.60***	−0.21
B(*a*)A	0.47	−0.07	−0.21	**−0.95****	0.33	**−0.69***	0.29	0.18	−0.36	**−0.69***	**−0.92****	**−0.53***	−0.37	**−0.79***	**0.60***	−0.21
CHR	**0.79****	**−0.67***	0.30	−0.47	−0.33	**−0.74***	**−0.56***	**−0.62***	−0.36	**−0.69***	**−0.92****	**−0.53***	−0.37	**−0.79***	**0.60***	−0.21
B(*b*)FA	−0.24	0.60	**−0.54***	−0.47	−0.33	**−0.74***	**−0.56***	**−0.62***	0.36	**−0.69***	**−0.92****	**−0.53***	−0.37	**−0.79***	**0.60***	−0.21
B(*k*)FA	0.47	−0.07	−0.21	**−0.95****	−0.33	**−0.74***	**−0.56***	**−0.62***	0.36	**−0.69***	**−0.92****	**−0.53***	−0.37	**−0.79***	**0.60***	−0.21
B(*j*)FA	0.47	−0.07	−0.21	**−0.95****	−0.33	**−0.74***	**−0.56***	**−0.62***	0.36	**−0.69***	**−0.92****	**−0.53***	−0.37	**−0.79***	**0.60***	−0.21
B(*e*)P	**−0.79****	**−0.67***	−0.30	0.47	−0.33	**−0.74***	**−0.56***	**−0.62***	0.36	**−0.69***	**−0.92****	**−0.53***	−0.37	**−0.79***	**0.60***	−0.21
B(*a*)P	0.47	−0.07	−0.21	**−0.95****	−0.33	**−0.74***	**−0.56***	**−0.62***	0.36	**−0.69***	**−0.92****	**−0.53***	−0.37	**−0.79***	**0.60***	−0.21
IP	0.47	−0.07	−0.21	**−0.95****	−0.33	**−0.74***	**−0.56***	**−0.62***	0.36	**−0.69***	**−0.92****	**−0.53***	−0.37	**−0.79***	**0.60***	−0.21
DB(*a*,*h*)A	−0.24	0.60	**−0.54***	−0.47	−0.33	**−0.74***	**−0.56***	**−0.62***	0.36	**−0.69***	**−0.92****	**−0.53***	−0.37	**−0.79***	**0.60***	−0.21
B(*g*,*h*,*i*)P	−0.24	0.60	**−0.54***	−0.47	−0.33	**−0.74***	**−0.56***	**−0.62***	0.36	**−0.69***	**−0.92****	**−0.53***	−0.37	**−0.79***	**0.60***	−0.21

The values are Spearman's correlation coefficients (ρ). Asterisks indicate statistical significance * ($P < 0.05$) and ** ($P \leq 0.001$). PAHs: polycyclic aromatic hydrocarbons.

Table 4
Associations of PM inorganic components with DNA replication and damage in the 100 μg/mL group cells.

Items	$PM_{10-2.5}$		$PM_{2.5-1}$		$PM_{1-0.2}$		$PM_{0.2}$	
	Sub G1/G0	DNA Tail-I	Sub G1/G0	DNA Tail-I	Sub G1/G0	DNA Tail-I	Sub G1/G0	DNA Tail-I
Ions	**0.95****	**−0.59***	0.47	**−0.58***	−0.57	**−0.94****	−0.47	−0.11
Na^+	**0.95****	**−0.59***	0.47	**−0.58***	−0.57	**−0.94****	0.47	**0.66***
NH_4^+	0.47	**−0.67***	−0.47	**0.58***	−0.57	**0.47***	**−0.95****	**−0.76****
K^+	**0.95****	**−0.59***	0.47	**−0.58***	−0.57	**−0.94****	0.47	**0.66***
Ca^{2+}	**−0.95****	**0.59***	**−0.95****	**0.84****	−0.57	**−0.94****	0.47	**0.66***
Cl^-	**0.95****	**−0.59***	0.47	**−0.58***	**0.95****	**0.47***	0.47	**0.66***
NO_3^-	0.47	**−0.67***	0.47	**−0.58***	**0.95****	**0.47***	0.47	**0.66***
SO_4^{2-}	**0.95****	**−0.59***	0.47	**−0.58***	−0.57	**−0.94****	−0.47	−0.11
TE	−0.47	**0.67***	**0.95****	**−0.84****	**0.95****	**0.47***	−0.47	−0.11
Al	−0.47	**0.67***	0.47	−0.26	0.57	**0.94****	**0.95****	**0.76****
Si	−0.47	**0.67***	**0.95****	**−0.84****	**0.95****	**0.47***	0.47	0.11
Cr	0.47	0.08	0.47	−0.26	**0.95****	**0.47***	−0.47	−0.11
Mn	−0.47	**0.67***	0.47	−0.26	0.57	**0.94****	0.47	**0.66***
Fe	−0.47	**0.67***	0.47	−0.26	**0.95****	**0.47***	0.47	**0.66***
Ni	0.47	0.08	**0.95****	**−0.84****	0.57	**−0.47***	0.47	**0.66***
Cu	−0.47	**0.67***	0.47	−0.26	0.57	**0.94****	0.47	0.11
Zn	0.47	0.08	0.47	−0.26	0.57	**0.94****	**0.95****	**0.76****
As	−0.47	**0.67***	0.47	−0.26	−0.57	**0.47***	−0.47	**−0.66***
Sr	−0.47	**0.67***	0.47	**−0.58***	0.57	**−0.47***	0.47	**0.66***
Cd	−0.47	**0.67***	−0.47	**0.58***	−0.57	**0.47***	−0.47	**−0.66***
Sn	0.47	0.08	0.47	−0.26	0.57	**0.94****	0.47	0.11
Sb	−0.47	**0.67***	0.47	−0.26	0.57	**0.94****	−0.47	**−0.66***
Ba	0.47	0.08	0.47	−0.26	0.57	**−0.47***	**0.95****	**0.76****
Pb	−0.47	**0.67***	−0.47	**0.58***	−0.57	**0.47***	−0.47	**−0.66***

The values are Spearman's correlation coefficients (ρ). Asterisks indicate statistical significance * ($P < 0.05$) and ** ($P \leq 0.001$). TE: total elements; DNA Tail-I: DNA Tail-Intensity.

samples were strongly correlated with nearly all the toxicological responses, and also with diverse toxicological endpoints. Our study provides novel and essential insights for subsequent studies on risk assessment of PM-induced toxicological endpoints and how these outcomes vary across PM of different sizes.

Ambient PM concentrations were comparatively high from December 2017 to March 2018 in Guangzhou; the average $PM_{2.5}$ concentration was 72 μg/m^3, which far exceeded air quality standard released by World Health Organization in 2021 (Who, 2021). The mean concentration of $PM_{2.5}$ in Guangzhou varies with the seasons, with the highest concentrations are observed in winter and the lowest in summer. Rainfall is the main reason for the low $PM_{2.5}$ concentration in summer (Griffith et al., 2015; Lai et al., 2016). High winter $PM_{2.5}$ concentrations are observed due to infrequent precipitation, which fails to clear aerosols that accumulate because of local emissions and the transfer of $PM_{2.5}$ from other cities (Fan et al., 2015; Gu and Yim, 2016). Evidence from epidemiological studies indicate that high levels of PM induced are associated with increased mortality in cardiopulmonary diseases in Guangzhou, despite the fact that PM concentrations in Guangzhou are comparatively low in China (Bhatia-Barnes et al., 2017; Li et al., 2021). Previous studies on PM have mainly focused on $PM_{2.5}$ and PM_{10}. In recent years, some studies indicated that $PM_{0.5}$ or the smaller particles may be the main cause of the adverse health effects of PM pollution (Feng et al., 2021a; Feng et al., 2021b; Guo et al., 2021; He et al., 2021; Meng et al., 2013; Yang et al., 2022a). At present, national monitoring data on atmospheric concentrations of small particles are lacking. Hence, further research on small particle sizes and their impact on human health is required to provide a basis for informing air quality standards.

PM composition is extremely complex and can induce a variety of toxicological effects. Similar to previous researches (Rönkkö et al., 2020;

Table 5
Associations of PM organic components PAHs with DNA replication and damage in the 100 μg/mL group cells.

Items	$PM_{10-2.5}$		$PM_{2.5-1}$		$PM_{1-0.2}$		$PM_{0.2}$	
	Sub G1/G0	DNA Tail-I	Sub G1/G0	DNA Tail-I	Sub G1/G0	DNA Tail-I	Sub G1/G0	DNA Tail-I
PAHs	0.47	0.08	0.47	−0.26	−0.57	**0.47***	0.47	0.11
NA	0.47	**−0.67***	**0.95****	**−0.84****	−0.57	**−0.94****	0.47	**0.66***
AC	**0.95****	**−0.59***	0.47	−0.26	−0.57	**−0.94****	**0.95****	**0.76****
ACL	−0.47	**0.67***	**0.95****	**−0.84****	0.57	**−0.47***	0.47	**0.66***
FL	**0.95****	**−0.59***	0.47	−0.26	−0.57	**−0.94****	−0.47	−0.11
PHE	**0.95****	**−0.59***	**0.95****	**−0.84****	−0.57	**0.47***	0.47	0.11
AN	0.47	0.08	**0.95****	**−0.84****	**−0.95****	**−0.47***	0.47	**0.66***
FA	0.47	0.08	**0.95****	**−0.84****	0.57	**0.94****	0.47	0.11
PY	0.47	0.08	**0.95****	**−0.84****	0.57	**0.94****	0.47	0.11
B(*a*)A	−0.47	**−0.67***	0.47	−0.26	−0.57	**0.47***	0.47	0.11
CHR	0.47	0.08	−0.47	**0.58***	−0.57	**0.47***	0.47	0.11
B(*b*)FA	**−0.95****	**0.59***	−0.47	**0.58***	−0.57	**0.47***	0.47	0.11
B(*k*)FA	−0.47	**0.67***	−0.47	**0.58***	−0.57	**0.47***	0.47	0.11
B(*j*)FA	−0.47	**0.67***	−0.47	**0.58***	−0.57	**0.47***	0.47	0.11
B(*e*)P	−0.47	0.08	−0.47	**0.58***	−0.57	**0.47***	0.47	0.11
B(*a*)P	−0.47	**0.67***	−0.47	**0.58***	−0.57	**0.47***	0.47	0.11
IP	−0.47	**0.67***	−0.47	**0.58***	−0.57	**0.47***	0.47	0.11
DB(*a*,*h*)A	**−0.95****	**0.59***	−0.47	**0.58***	−0.57	**0.47***	0.47	0.11
B(*g*,*h*,*i*)P	**−0.95****	**0.59***	−0.47	**0.58***	−0.57	**0.47***	0.47	0.11

The values are Spearman's correlation coefficients (ρ). Asterisks indicate statistical significance * ($P < 0.05$) and ** ($P \leq 0.001$). PAHs: polycyclic aromatic hydrocarbons.

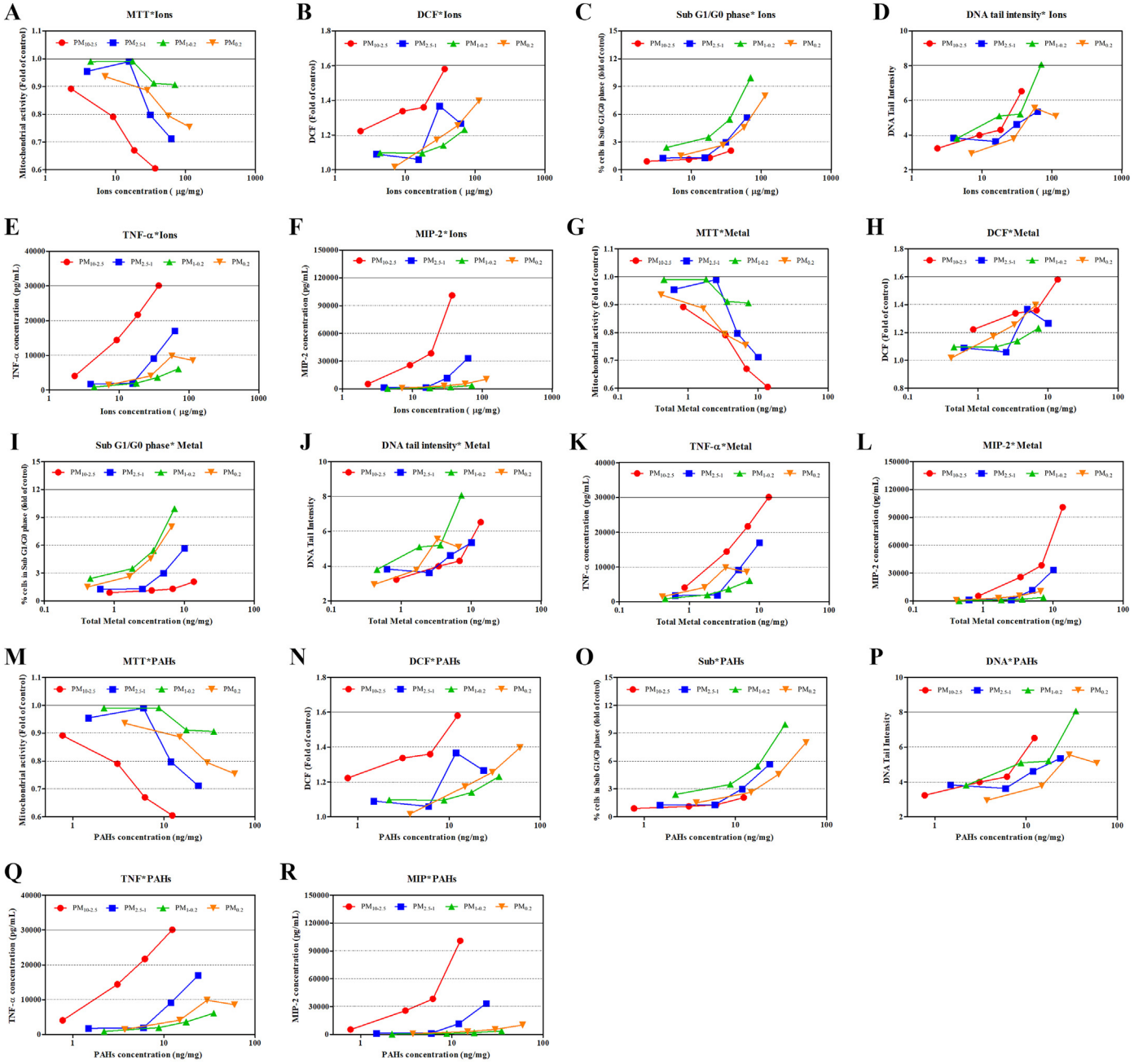

Fig. 4. Associations of PM components (total ions, metals, PAHs) with toxicological endpoints in size-segregated particulate samples.

Rönkkö et al., 2018a), our results showed that the larger-diameter PM contained more metallic elements, the smaller-diameter PM contained more ions and PAHs. In this study, SO_4^{2-} and NO_3^- were relatively enriched ions across the four size-segregated PM samples. Long-term exposure to $PM_{2.5}$-NO_3^- and $PM_{2.5}$-SO_4^{2-} led to an impaired respiratory system in C57BL/6 mice, with toxicological effects of $PM_{2.5}$-SO_4^{2-} considerably weaker than $PM_{2.5}$-NO_3^- (Zhang et al., 2021). A nationwide case-control study in Denmark revealed that exposure to PM-NO_3^- was related to an increased persistent wheezing and asthma (Holst et al., 2020), while the effect of PM-SO_4^{2-} is equivocal (Reiss et al., 2007). PM-NO_3^- and PM-SO_4^{2-} were positive regulators of inflammation and oxidative damage in this study. However, in a study of PM toxicity in Helsinki, it was found that PM-NO_3^- and PM-SO_4^{2-} negatively regulate the inflammatory effect of large particles, and positively regulate the inflammatory effect of small particles (Jalava et al., 2015a). Therefore, toxic effects caused by similar components in PM can vary geographically. In this study, K was the amplest metallic element in $PM_{0.2}$, while Si was the dominant metallic element in $PM_{10–2.5}$, $PM_{2.5–1}$, and $PM_{1–0.2}$., K is mainly emitted from biomass burning, and is closely related to cardiovascular diseases, such as high blood pressure, stroke and coronary heart disease (Weaver, 2013; Yang et al., 2017). The main sources of Si are soil dust and traffic exhaust, and chronic occupational exposure to Si via inhalation give rise to severe respiratory diseases (Bhattacharjee et al., 2016; Reff et al., 2009). Most single PAHs were more prevalent in the smaller-diameter PM, while FA was relatively high in all PM samples in this study. Toxicological evidence suggests that FA is a potent mutagen and carcinogen, is not easily degraded in the environment, it easily deposited in soil, and its cytotoxicity is stronger than B (*a*)A in seven species of marine algae (Ben et al., 2012; Kadri et al., 2017). Therefore, the environmental hazards of FA deserve more attention.

The sources of PM are numerous and are easily influenced by human activities and environmental policies. PM samples in this study were collected at the North campus of Sun Yat-sen University. There are several hospitals

and schools nearby, coupled with residential buildings and restaurants around the campus at the major and minus roads. Furthermore, the Guangzhou Petrochemical Company is roughly 19 km from the PM sampling point in this study. These factors inevitably contribute to excessive vehicle exhausts, and cooking and fuel combustion. In addition, the weather in Guangzhou from December 2017 to March 2018 was less rainy and dry; this coupled with dust carried by vehicles, led to soil dust being the main contributing source to $PM_{10–2.5}$, which could also explain why Si was the most abundant metals in $PM_{10–2.5}$ (Reff et al., 2009). Indoor heating that utilizes coal-burning in winter in northern Chinese cities resulted in a large fraction of $PM_{2.5–1}$ and $PM_{1–0.2}$ coming from coal combustion in this study. The main sources of $PM_{0.2}$ were biomass burning/petrochemical and traffic exhaust in this study. Biomass burning is mainly classified into four types in China: forest fire, wood and straw combustion as fuel, agricultural straw open burning, and co-firing with coal or municipal solid waste (Chen et al., 2017). There are still many rural households in the Pearl River Delta (PRD) and surrounding areas in Guangdong Province, which use biofuels (agricultural residues and firewood) as domestic fuel for cooking (Zhang et al., 2010). Remarkably, the contribution of biomass burning to $PM_{2.5}$ has been confirmed in Guangzhou via organic tracers (acetonitrile and levoglucosan), in which the frequency of $PM_{2.5}$ pollution events involved biomass burning for suburban and downtown areas was 100 % and 58 %, respectively (Wang et al., 2007). For example, while the annual $PM_{2.5}$-SO_4^{2-} and $PM_{2.5}$-NO_3^- concentrations in urban Guangzhou were reduced from 2010 to 2014 because of the implementation of high-efficiency desulfurization and dust removal technology for large and medium-sized industrial boilers in Guangdong Province (Tao et al., 2017), $PM_{2.5}$-SO_4^{2-} and $PM_{2.5}$-NO_3^- concentrations in Guangzhou suburbs were elevated due to biomass burning, secondary aerosol formation, and long-range transport form PRD region and the northern provinces of Hunan and Jiangxi (Lai et al., 2016). The importance of traffic exhaust to the formation of smaller-diameter PM has been verified (Jalava et al., 2007; Papa et al., 2021). Vehicular exhaust, coal-fired power generation and incomplete combustion of coal and petrol are major sources of PAHs (Famiyeh et al., 2021). In particular, $PM_{0.2}$ showed the highest fractions of total contents of PAHs and ions.

The link between oxidative stress and PM-induced lung disease has been well established (Li et al., 2008). Toxicological analysis revealed that, among four different-sized PM samples collected from Nanjing, $PM_{10–2.5}$ led to the greatest oxidative stress in human adenocarcinomic alveolar basal epithelial cells (Rönkkö et al., 2018b). In this study, $PM_{10–2.5}$ resulted in the largest oxidative stress, thereby decreasing cell mitochondrial activity and increasing intracellular oxidative potential. Organic and metallic components could lead to direct oxidation from PM, which would result in oxidative stress via consumption of antioxidants through a series of biochemical reactions (Ghio et al., 2012). However, the impact of specific PM components on oxidative stress remains unclear. It has been shown that transition metals may contribute to the induction oxidative stress via generation of reactive oxygen species (ROS) (Li et al., 2008). One study of oil fly ash solution, consisting of transition metals Ni (10.1 %), V (32.4 %) and Fe (57.5 %), revealed that exposure to oil fly ash increased generation of intracellular ROS in a concentration- and time-dependent manner in A549 cells (Di Pietro et al., 2009). In addition to ROS generation, numerous studies have demonstrated that exposure to PM-metals, such as V, Zn, Ni, Pb, Hg, and As, decreased glutathione levels in cells and tissues, which resulted in oxidative stress (Stohs and Bagchi, 1995). Mitochondria are a primary source of intracellular ROS, and mitochondrial respiration is tightly regulated by redox-mediated processes that involve glutathione and cysteine thiol (Samet et al., 2020). Environmental PM-metals, including As, Hg, V, Pb, Zn, and Cd, were found to impair mitochondrial function (Samet et al., 2020). In this study, intracellular oxidation potential (DCF) and mitochondrial activity (MTT) were negatively correlated in most PM samples, with the strongest association ($P < 0.001$, $\rho = -0.806$) observed for $PM_{10–2.5}$. Nevertheless, increased PM-PAHs did not lead to more pronounced oxidative stress. In Taiyuan and Guangzhou, the intracellular oxidative stress induced by winter $PM_{2.5}$-PAHs with higher concentrations was not significantly more than that of summer $PM_{2.5}$-PAHs (Song et al., 2020). In this study, PM-metals (Cr, Ni, Sn, Zn, and Ba) and PM-PAHs (total PAHs, AN, FA, PY, CHR, B(*e*)P) were correlated with both DCF and MTT in $PM_{10–2.5}$. However, associations between PM-ions and MTT or DCF were not found in $PM_{10–2.5}$, but they were observed in other PM, which may account for the lowest ions in $PM_{10–2.5}$. It has been reported that water-soluble ions of PM, such as SO_4^{2-} and NO_3^-, could lead to potential toxicity mediated by PM, with the SO_4^{2-}/NO_3^- mixture resulting in rare gene expression patterns (Park et al., 2022). In addition, we found that strong oxidative stress did not destroy cell membrane integrity, and a strong correlation between oxidative stress and cell membrane integrity was only seen in $PM_{1–0.2}$. Importantly, Cr, CHR, and B(*e*)P were strongly associated with DCF, while AN was closely related to MTT in all PM samples. Specifically, Zn, Sn, Ba, CHR, and B(*e*)P, were strongly correlated with MTT only in $PM_{10–2.5}$. An epidemiological study observed higher levels of oxidative stress in shipyard welders exposed to metal fumes and PAHs, with a strong correlation between urinary metal (Cr and Cd) and oxidative stress levels (Lai et al., 2020). Therefore, $PM_{10–2.5}$ exerted the strongest oxidative effect probably because of a higher content of metallic elements. Future studies still need to investigate how these PM components react individually or jointly to induce oxidative stress.

Numerous toxicological studies have confirmed the role of inflammation in PM-mediated diseases (Arias-Pérez et al., 2020). TNF-α, produced mainly by immune cells, is a powerful proinflammatory cytokine involved in the innate immune response (Zelová and Hošek, 2013). TNF can act as a regulator of ROS generation, and interaction between TNF and ROS is observed in inflammatory diseases, such as inflammatory bowel disease, systemic lupus erythematosus, and rheumatoid arthritis (Blaser et al., 2016). Therefore, high expression levels of TNF could be accompanied by increased ROS generation. TNF-α also functions as an effective activator of chemokine expression in immune and non-immune cells (Driscoll, 2000). Chemokine MIP-2 plays a significant role in regulating inflammation caused by particles such as quartz and crocidolite in rodent lungs, and MIP-2 expression can be mediated by transcription factor NF-kappa B and PM-induced oxidative stress (Driscoll, 2000). In this study, $PM_{10–2.5}$ resulted in the greatest expression of TNF-α and MIP-2. Moreover, it has been proven that PM-metals exert proinflammatory responses, and ROS production induced by transition metals, such as Fe, V, Cr, Ni, Co, and Cu, may play a vital role in this effect (Li et al., 2008). It has been demonstrated that metals, ions and PAHs of PM induce inflammatory responses and reduce cell survival (Kermani et al., 2021; Zhang et al., 2021). Nevertheless, for most PM samples in this study, total ions and metals, and most single ions, metals and PAHs were positively correlated with TNF-α and/or MIP-2 expression, while TNF-α/MIP-2 expression was not associated with total PAHs. We also found that no association between single metals and TNF-α expression, while the strongest correlations between most single metals and MIP-2 expression were mostly observed in $PM_{10–2.5}$. Furthermore, some components (NH_4^+, Sr, Cd, Pb) and organic components (NA and ACL) were strongly connected with MIP-2 expression, whereas some PAHs [PHE, B(*b*)FA, DB(*a*,*h*)A, B(*g*,*h*,*i*)P] correlated with TNF-α expression across the four size-segregated PM samples in this study. Toxicological effects cannot be explained simply by PM composition, because combined toxicological effects of multiple chemicals are difficult to assess. The aforementioned study by Lai et al. that demonstrated increased oxidative stress in shipyard welders due to urinary metal and PAH exposure, suggested that elevated levels of oxidative stress may lead to increased secretion of inflammatory cytokines (serum IL-6 and TNF-α) (Lai et al., 2020). Subsequently, we found that markers of oxidative stress were associated with inflammatory mediators (TNF-α and MIP-2) in most PM samples with the strongest correlation in $PM_{10–2.5}$. Therefore, oxidative stress is an essential step for an upregulated immune response observed for $PM_{10–2.5}$, and the role of transition metals in this process cannot be ignored.

Induction of DNA damage and alterations of the cell cycle has previously been demonstrated following environmental PM exposure (Rönkkö

et al., 2018b). In this study, an elevated Sub-G1/G0 population was observed for most PM samples, with the greatest effect seen with exposure to $PM_{1-0.2}$. Increased Sub-G1/G0 population in RAW264.7 cells suggests DNA damage and degradation, and apoptosis induced by excessive DNA repair capacity. Genotoxicity was seen in all PM samples in this study, with the most evident DNA damage occurring in $PM_{1-0.2}$. Interestingly, $PM_{10-2.5}$ caused high DNA tail intensity but did not upregulate the Sub-G1/G0 population, which indicates that $PM_{10-2.5}$ may lead to transient DNA damage and non-extensive DNA degradation. Previously, A549 cells exposed $PM_{10-2.5}$ or $CaSO_4$ particles also generated distinct genotoxicity and oxidative stress with inconspicuous cell cycle alteration due to elevated ROS generation (Könczöl et al., 2012; Rönkkö et al., 2018b). Yet, evidence indicates that increased oxidative stress leads to oxidative DNA damage, and that formation of oxidative DNA adducts induced by interactions between DNA and ROS, such as 8-oxoguanine and 8-hydroxy-2-deoxyguanosine, likely results in genotoxicity (Valavanidis et al., 2013). Furthermore, we did not find a strong correlation between the destruction of cell membrane integrity and high Sub-G1/G0 population in RAW264.7 cells exposed to $PM_{1-0.2}$ or $PM_{0.2}$. Similar findings were observed in A549 cells exposed to different-sized PM in Nanjing (Rönkkö et al., 2018b). The importance of PAHs on genotoxicity and cell cycle alteration with exposure to PM has been demonstrated in human bronchial epithelial BEAS-2B cells (Abbas et al., 2019). Additionally, PAH-DNA adducts, generated by the PAH-DNA binding, greatly influence genotoxicity upon PM exposure (Quezada-Maldonado et al., 2021). In this study, $PM_{0.2}$ with the highest PAH contents did not cause the most significant DNA lesion and cell cycle alterations, but $PM_{1-0.2}$ did. Experimental evidence suggests that PAH mixtures exert the lack of additivity and inhibitory effects on genotoxicity in A549 cells (Genies et al., 2016). Moreover, in this study, a positive association between genotoxicity and cell cycle effects was observed for $PM_{1-0.2}$ and $PM_{0.2}$, which suggests that increased Sub-G1/G0 population might be caused by DNA damage-induced apoptosis. We found that the majority of single inorganic components were not associated with increased Sub-G1/G0 population, but were linked with genotoxicity in most PM samples. Furthermore, all inorganic components were associated with a genotoxic response induced by $PM_{1-0.2}$, and NO_3^- ($\rho = 0.95$), Cr ($\rho = 0.95$), and Fe ($\rho = 0.95$) were positively associated with DNA damage only in $PM_{1-0.2}$. Cr and Fe belong to transition metals, and have been demonstrated to lead to intracellular DNA damage (Terpilowska and Siwicki, 2018). However, in this study, several organic components only correlated with cell cycle effects in a few PM samples, while most organic components were connected with genotoxic effects for most PM samples. Only AN ($\rho = -0.95$) was associated with elevated Sub-G1/G0 population, while all PAHs were associated with DNA tail intensity in $PM_{1-0.2}$ in this study. It has been previously demonstrated that total PAHs ($\rho = 0.512$), B(*a*)P ($\rho = 0.512$), B(*k*)FA ($\rho = 0.816$), Al ($\rho = 0.706$), Cl^- ($\rho = 0.732$), NO_3^- ($\rho = 0.791$), and Mn ($\rho = 0.571$) were related to genotoxicity in A549 cells exposed to $PM_{1-0.2}$ (Rönkkö et al., 2018a). Here, total PAHs, B(*a*)P, B(*k*)FA, Al, Cl^-, NO_3^-, Mn also displayed associations with genotoxicity in RAW264.7 cells exposed to $PM_{1-0.2}$, while FA, PY, Cu, Zn, Ba showed more stronger positive correlations with $PM_{1-0.2}$ induced genotoxicity. This apparent difference may be caused by variation of PM components being collected at different times and locations. In addition to the identified components, the unidentified components of PM may exert complex toxicological effects as well. Therefore, future studies should utilize innovate experimental methods to discover unidentified chemical species, and investigate interactions of PM components on cellular responses.

The current study has several strengths. First, the main emission sources of four size-segregated PM were analyzed and the contributions of emission sources to PM composition was assessed. Second, we measured, compared and correlated toxicological effects in four size-segregated PM, providing insights into the adverse health effects experienced by individuals upon exposure to air pollution. Third, associations between single composition and various toxicological endpoints were analyzed for all PM samples, this provides a platform for further studies and the development of specialized health risk assessments for key chemicals in the atmosphere. However, we did not simulate real ambient human PM exposure, and cannot fully evaluate the overall negative health effects caused by the different PM sizes. Additionally, the generally high ion concentrations that were detected in this study were predominantly caused by differences in calculation and calibration methods. Although a strong association was observed between oxidative stress and genotoxicity in RAW264.7 cells exposed to PM, the contribution of oxidative stress to genotoxicity remains undefined, and further studies are needed to investigate oxidative DNA damage to better understand the underlying mechanisms by which oxidative stress regulates genotoxicity.

5. Conclusions

$PM_{10-2.5}$ and $PM_{1-0.2}$ concentrations were high in four size-segregated PM samples collected form Guangzhou. The larger-diameter PM contained more metals, and fewer ions and PAHs, while the opposite was observed for the smaller-diameter PM. Soil dust, coal combustion and biomass burning/petrochemical were the major contributing sources to PM. Traffic exhaust, soil dust, and biomass burning/petrochemical were the main sources of PAHs, metals and ions, respectively. $PM_{10-2.5}$ exposure resulted in the strongest oxidative stress and inflammatory responses in RAW264.7 cells, while $PM_{1-0.2}$ exposure led to the most increase in Sub-G1/G0 population, loss of cell membrane integrity, and genotoxicity. Moderate-to-strong associations were found between most single chemical components and almost all toxicological effects as well as between various toxicological endpoints in the four size-segregated PM categories. Our findings provide novel and unique insight into various size-segregated PM-induced toxicological effects in cells and identify chemical components of PM that play a key role in adverse intracellular responses.

Supplementary data to this article can be found online at https://doi.org/10.1016/j.scitotenv.2022.161092.

CRediT authorship contribution statement

Mo Yang: Conceptualization, Methodology, Validation, Formal analysis, Investigation, Writing – original draft, Writing – review & editing, Resources, Data curation, Supervision. **Hui-Xian Zeng:** Conceptualization, Methodology, Validation, Formal analysis, Investigation, Writing – original draft, Writing – review & editing, Supervision. **Xin-Feng Wang:** Methodology, Formal analysis, Investigation, Writing – review & editing. **Henri Hakkarainen:** Methodology, Writing – review & editing. **Ari Leskinen:** Methodology, Writing – review & editing. **Mika Komppula:** Methodology. **Marjut Roponen:** Methodology. **Qi-Zhen Wu:** Methodology, Data curation. **Shu-Li Xu:** Methodology, Data curation. **Li-Zi Lin:** Formal analysis, Investigation. **Ru-Qing Liu:** Formal analysis, Investigation, Funding acquisition. **Li-Wen Hu:** Formal analysis, Investigation, Funding acquisition. **Bo-Yi Yang:** Formal analysis, Investigation, Funding acquisition. **Xiao-Wen Zeng:** Conceptualization, Methodology, Funding acquisition. **Guang-Hui Dong:** Conceptualization, Methodology, Validation, Writing – original draft, Writing – review & editing, Funding acquisition, Resources, Supervision. **Pasi Jalava:** Conceptualization, Methodology, Validation, Writing – original draft, Writing – review & editing, Funding acquisition, Resources, Supervision.

Data availability

Data will be made available on request.

Declaration of Competing Interest

The authors declare that they have no known competing financial interests or personal relationships that could have appeared to influence the work reported in this paper.

Acknowledgements

This work was supported by the National Key Research and Development Program of China (No. 2018YFC1004300, 2018YFC1004301, 2018YFE0106900), National Natural Science Foundation of China (No. 82103823, 81872583, 82073502, 81872582, M-0420), the Natural Science Foundation of Guangdong Province (No. 2021B1515020015, 2019A050510017, 2017A090905042), Academy of Finland (No. 287982).

References

Abbas, I., Badran, G., Verdin, A., Ledoux, F., Roumie, M., Lo Guidice, J.-M., et al., 2019. In vitro evaluation of organic extractable matter from ambient PM2.5 using human bronchial epithelial BEAS-2B cells: cytotoxicity, oxidative stress, pro-inflammatory response, genotoxicity, and cell cycle deregulation. Environ. Res. 171, 510–522.

Arias-Pérez, R.D., Taborda, N.A., Gómez, D.M., Narvaez, J.F., Porras, J., Hernandez, J.C., 2020. Inflammatory effects of particulate matter air pollution. Environ. Sci. Pollut. Res. Int. 27, 42390–42404.

Arruti, A., Fernández-Olmo, I., Irabien, A., 2011. Impact of the global economic crisis on metal levels in particulate matter (PM) at an urban area in the Cantabria region (Northern Spain). Environ. Pollut. 159, 1129–1135.

Ben, O.H., Leboulanger, C., Le Floc'H, E., Mabrouk, H.H., Hlaili, A.S., 2012. Toxicity of benz (a)anthracene and fluoranthene to marine phytoplankton in culture: does cell size really matter? J. Hazard. Mater. 243, 204–211.

Bhatia-Barnes, J., Gupta, M., Bell, C., Samuels, J., 2017. Abstract P222: prevalence of hypotension in adolescents. Hypertension 70 AP222-AP222.

Bhattacharjee, P., Paul, S., Bhattacharjee, P., 2016. Risk of occupational exposure to asbestos, silicon and arsenic on pulmonary disorders: understanding the genetic-epigenetic interplay and future prospects. Environ. Res. 147, 425–434.

Blaser, H., Dostert, C., Mak, T.W., Brenner, D., 2016. TNF and ROS crosstalk in inflammation. Trends Cell Biol. 26, 249–261.

Chen, N., Xu, L., 2017. Relationship between air quality and economic development in the provincial capital cities of China. Environ. Sci. Pollut. Res. 24, 2928–2935.

Chen, J., Li, C., Ristovski, Z., Milic, A., Gu, Y., Islam, M.S., et al., 2017. A review of biomass burning: emissions and impacts on air quality, health and climate in China. Sci. Total Environ. 579, 1000–1034.

Di Pietro, A., Visalli, G., Munaò, F., Baluce, B., La Maestra, S., Primerano, P., et al., 2009. Oxidative damage in human epithelial alveolar cells exposed in vitro to oil fly ash transition metals. Int. J. Hyg. Environ. Health 212, 196–208.

Driscoll, K.E., 2000. TNFalpha and MIP-2: role in particle-induced inflammation and regulation by oxidative stress. Toxicol. Lett. 112–113, 177–183.

Famiyeh, L., Chen, K., Xu, J., Sun, Y., Guo, Q., Wang, C., et al., 2021. A review on analysis methods, source identification, and cancer risk evaluation of atmospheric polycyclic aromatic hydrocarbons. Sci. Total Environ. 789, 147741.

Fan, Q., Lan, J., Liu, Y., Wang, X., Chan, P., Hong, Y., et al., 2015. Process analysis of regional aerosol pollution during spring in the Pearl River Delta regionChina. Atmospheric Environment 122, 829–838.

Feng, D., Cao, K., He, Z.-Z., Knibbs, L.D., Jalaludin, B., Leskinen, A., et al., 2021a. Short-term effects of particle sizes and constituents on blood biomarkers among healthy young adults in GuangzhouChina. Environmental Science & Technology 55, 5636–5647.

Feng, D., Cao, K., Zou, J., Bloom, M.S., Lin, S., Yu, Y., et al., 2021b. Associations between size-fractioned particulate matter and left ventricular voltage: a panel study among healthy young adults in southern China. Atmos. Environ. 254, 118395.

Genies, C., Jullien, A., Lefebvre, E., Revol, M., Maitre, A., Douki, T., 2016. Inhibition of the formation of benzo[a]pyrene adducts to DNA in A549 lung cells exposed to mixtures of polycyclic aromatic hydrocarbons. Toxicol. in Vitro 35, 1–10.

Ghio, A.J., Carraway, M.S., Madden, M.C., 2012. Composition of air pollution particles and oxidative stress in cells, tissues, and living systems. J. Toxicol. Environ. Health B Crit. Rev. 15, 1–21.

Griffith, S.M., Huang, X.H.H., Louie, P.K.K., Yu, J.Z., 2015. Characterizing the thermodynamic and chemical composition factors controlling PM2.5 nitrate: insights gained from two years of online measurements in Hong Kong. Atmos. Environ. 122, 864–875.

Gu, Y., Yim, S.H.L., 2016. The air quality and health impacts of domestic trans-boundary pollution in various regions of China. Environ. Int. 97, 117–124.

Guo, P.Y., He, Z.Z., Jalaludin, B., Knibbs, L.D., Leskinen, A., Roponen, M., et al., 2021. Short-term effects of particle size and constituents on blood pressure in healthy young adults in Guangzhou, China. J. Am. Heart Assoc. 10, e019063.

Hakkarainen, H., Salo, L., Mikkonen, S., Saarikoski, S., Aurela, M., Teinilä, K., et al., 2022. Black carbon toxicity dependence on particle coating: measurements with a novel cell exposure method. Sci. Total Environ. 838, 156543.

He, Z.-Z., Guo, P.-Y., Xu, S.-L., Zhou, Y., Jalaludin, B., Leskinen, A., et al., 2021. Associations of particulate matter sizes and chemical constituents with blood lipids: a panel study in GuangzhouChina. Environmental Science & Technology 55, 5065–5075.

Holst, G.J., Pedersen, C.B., Thygesen, M., Brandt, J., Geels, C., Bønløkke, J.H., et al., 2020. Air pollution and family related determinants of asthma onset and persistent wheezing in children: nationwide case-control study. BMJ 370, m2791.

Jalava, P.I., Salonen, R.O., Hälinen, A.I., Penttinen, P., Pennanen, A.S., Sillanpää, M., et al., 2006. In vitro inflammatory and cytotoxic effects of size-segregated particulate samples collected during long-range transport of wildfire smoke to Helsinki. Toxicol. Appl. Pharmacol. 215, 341–353.

Jalava, P.I., Salonen, R.O., Pennanen, A.S., Sillanpää, M., Hälinen, A.I., Happo, M.S., et al., 2007. Heterogeneities in inflammatory and cytotoxic responses of RAW 264.7 macrophage cell line to urban air coarse, fine, and ultrafine particles from six european sampling campaigns. Inhal. Toxicol. 19, 213–225.

Jalava, P.I., Happo, M.S., Huttunen, K., Sillanpää, M., Hillamo, R., Salonen, R.O., et al., 2015a. Chemical and microbial components of urban air PM cause seasonal variation of toxicological activity. Environ. Toxicol. Pharmacol. 40, 375–387.

Jalava, P.I., Wang, Q., Kuuspalo, K., Ruusunen, J., Hao, L., Fang, D., et al., 2015b. Day and night variation in chemical composition and toxicological responses of size segregated urban air PM samples in a high air pollution situation. Atmos. Environ. 120, 427–437.

Kadri, T., Rouissi, T., Kaur, B.S., Cledon, M., Sarma, S., Verma, M., 2017. Biodegradation of polycyclic aromatic hydrocarbons (PAHs) by fungal enzymes: a review. J. Environ. Sci. (China) 51, 52–74.

Kermani, M., Rahmatinia, T., Oskoei, V., Norzaee, S., Shahsavani, A., Farzadkia, M., et al., 2021. Potential cytotoxicity of trace elements and polycyclic aromatic hydrocarbons bounded to particulate matter: a review on in vitro studies on human lung epithelial cells. Environ. Sci. Pollut. Res. Int. 28, 55888–55904.

Könczöl, M., Goldenberg, E., Ebeling, S., Schäfer, B., Garcia-Käufer, M., Gminski, R., et al., 2012. Cellular uptake and toxic effects of fine and ultrafine metal-sulfate particles in human A549 lung epithelial cells. Chem. Res. Toxicol. 25, 2687–2703.

Lai, S., Zhao, Y., Ding, A., Zhang, Y., Song, T., Zheng, J., et al., 2016. Characterization of PM2.5 and the major chemical components during a 1-year campaign in rural Guangzhou, southern China. Atmos. Res. 167, 208–215.

Lai, C.H., Chou, C.C., Chuang, H.C., Lin, G.J., Pan, C.H., Chen, W.L., 2020. Receptor for advanced glycation end products in relation to exposure to metal fumes and polycyclic aromatic hydrocarbon in shipyard welders. Ecotoxicol. Environ. Saf. 202, 110920.

Lee, H.Y., Yang, H.K., Song, H.J., Chang, H.J., Kang, J.Y., Lee, S.H., et al., 2019. Metabolic health is more closely associated with decrease in lung function than obesity. PloS one 14, e0209575.

Li, N., Xia, T., Nel, A.E., 2008. The role of oxidative stress in ambient particulate matter-induced lung diseases and its implications in the toxicity of engineered nanoparticles. Free Radic. Biol. Med. 44, 1689–1699.

Li, M., Wang, X., Lu, C., Li, R., Zhang, J., Dong, S., et al., 2020. Nitrated phenols and the phenolic precursors in the atmosphere in urban JinanChina. Sci Total Environ 714, 136760.

Li, B., Yang, J., Dong, H., Li, M., Cai, D., Yang, Z., et al., 2021. PM(2.5) constituents and mortality from a spectrum of causes in Guangzhou, China. Ecotoxicol. Environ. Saf. 222, 112498.

Longhin, E.M., Mantecca, P., Gualtieri, M., 2020. Fifteen years of airborne particulates in vitro toxicology in Milano: lessons and perspectives learned. Int. J. Mol. Sci. 21.

Meng, X., Ma, Y., Chen, R., Zhou, Z., Chen, B., Kan, H., 2013. Size-fractionated particle number concentrations and daily mortality in a chinese city. Environ. Health Perspect. 121, 1174–1178.

Papa, G., Capitani, G., Capri, E., Pellecchia, M., Negri, I., 2021. Vehicle-derived ultrafine particulate contaminating bees and bee products. Sci. Total Environ. 750, 141700.

Park, S., Ku, J., Lee, S.-M., Hwang, H., Lee, N., Kim, H., et al., 2022. Potential toxicity of inorganic ions in particulate matter: ion permeation in lung and disruption of cell metabolism. Sci. Total Environ. 824, 153818.

Polissar, A.V., Hopke, P.K., Paatero, P., Malm, W.C., Sisler, J.F., 1998. Atmospheric aerosol over Alaska: 2Elemental composition and sources. Journal of Geophysical Research Atmospheres 103, 19045–19057.

Quezada-Maldonado, E.M., Sánchez-Pérez, Y., Chirino, Y.I., García-Cuellar, C.M., 2021. Airborne particulate matter induces oxidative damage, DNA adduct formation and alterations in DNA repair pathways. Environ. Pollut. 287, 117313.

Reff, A., Bhave, P.V., Simon, H., Pace, T.G., Pouliot, G.A., Mobley, J.D., et al., 2009. Emissions inventory of PM2.5 trace elements across the United States. Environ. Sci. Technol. 43, 5790–5796.

Reiss, R., Anderson, E.L., Cross, C.E., Hidy, G., Hoel, D., McClellan, R., et al., 2007. Evidence of health impacts of sulfate-and nitrate-containing particles in ambient air. Inhal. Toxicol. 19, 419–449.

Rönkkö, T.J., Jalava, P.I., Happo, M.S., Kasurinen, S., Sippula, O., Leskinen, A., et al., 2018a. Emissions and atmospheric processes influence the chemical composition and toxicological properties of urban air particulate matter in NanjingChina. Science of The Total Environment 639, 1290–1310.

Rönkkö, T.J., Jalava, P.I., Happo, M.S., Kasurinen, S., Sippula, O., Leskinen, A., et al., 2018b. Emissions and atmospheric processes influence the chemical composition and toxicological properties of urban air particulate matter in NanjingChina. Sci Total Environ 639, 1290–1310.

Rönkkö, T.J., Hirvonen, M.R., Happo, M.S., Leskinen, A., Koponen, H., Mikkonen, S., et al., 2020. Air quality intervention during the Nanjing youth olympic games altered PM sources, chemical composition, and toxicological responses. Environ. Res. 185, 109360.

Rönkkö, T.J., Hirvonen, M.R., Happo, M.S., Ihantola, T., Hakkarainen, H., Martikainen, M.V., et al., 2021. Inflammatory responses of urban air PM modulated by chemical composition and different air quality situations in NanjingChina. Environ Res 192, 110382.

Samet, J.M., Chen, H., Pennington, E.R., Bromberg, P.A., 2020. Non-redox cycling mechanisms of oxidative stress induced by PM metals. Free Radic. Biol. Med. 151, 26–37.

Song, Y., Zhang, Y., Li, R., Chen, W., Chung, C.K.A., Cai, Z., 2020. The cellular effects of PM2.5 collected in chinese Taiyuan and Guangzhou and their associations with polycyclic aromatic hydrocarbons (PAHs), nitro-PAHs and hydroxy-PAHs. Ecotoxicol. Environ. Saf. 191, 110225.

Stohs, S.J., Bagchi, D., 1995. Oxidative mechanisms in the toxicity of metal ions. Free Radic. Biol. Med. 18, 321–336.

Tao, J., Zhang, L., Cao, J., Zhong, L., Chen, D., Yang, Y., et al., 2017. Source apportionment of PM(2.5) at urban and suburban areas of the Pearl River Delta region, South China - with emphasis on ship emissions. Sci. Total Environ. 574, 1559–1570.

Terpilowska, S., Siwicki, A.K., 2018. Interactions between chromium(III) and iron(III), molybdenum(III) or nickel(II): cytotoxicity, genotoxicity and mutagenicity studies. Chemosphere 201, 780–789.

Valavanidis, A., Vlachogianni, T., Fiotakis, K., Loridas, S., 2013. Pulmonary oxidative stress, inflammation and cancer: respirable particulate matter, fibrous dusts and ozone as major causes of lung carcinogenesis through reactive oxygen species mechanisms. Int. J. Environ. Res. Public Health 10, 3886–3907.

Velali, E., Papachristou, E., Pantazaki, A., Besis, A., Samara, C., Labrianidis, C., et al., 2018. In vitro cellular toxicity induced by extractable organic fractions of particles exhausted from urban combustion sources - role of PAHs. Environ. Pollut. 243, 1166–1176.

Verma, V., Salana, S., 2022. AS&T virtual collection: Toxicity of ambient particulate matter-impact of chemical composition, emission sources and atmospheric processes. Aerosol Sci. Technol. 56, 403–404.

Wang, Q., Shao, M., Liu, Y., William, K., Paul, G., Li, X., et al., 2007. Impact of biomass burning on urban air quality estimated by organic tracers: Guangzhou and Beijing as cases. Atmos. Environ. 41, 8380–8390.

Weaver, C.M., 2013. Potassium and health. Adv Nutr 4, 368S–377S.

Who, 2021. WHO Global Air Quality Guidelines: Particulate Matter (PM2.5 and PM10), Ozone, Nitrogen Dioxide, Sulfur Dioxide and Carbon Monoxide. World Health Organization, Geneva.

Yang, W., Zhu, Y., Cheng, W., Sang, H., Yang, H., Chen, H., 2017. Characteristics of particulate matter emitted from agricultural biomass combustion. Energy Fuel 31, 7493–7501.

Yang, M., Jalava, P., Hakkarainen, H., Roponen, M., Leskinen, A., Komppula, M., et al., 2022a. Fine and ultrafine airborne PM influence inflammation response of young adults and toxicological responses in vitro. Sci. Total Environ. 836, 155618.

Yang, M., Jalava, P., Wang, X.-F., Bloom, M.S., Leskinen, A., Hakkarainen, H., et al., 2022b. Winter and spring variation in sources, chemical components and toxicological responses of urban air particulate matter samples in GuangzhouChina. Science of The Total Environment 845, 157382.

Zelová, H., Hošek, J., 2013. TNF-α signalling and inflammation: interactions between old acquaintances. Inflamm. Res. 62, 641–651.

Zhang, Z., Engling, G., Lin, C.-Y., Chou, C.C.K., Lung, S.-C.C., Chang, S.-Y., et al., 2010. Chemical speciation, transport and contribution of biomass burning smoke to ambient aerosol in Guangzhou, a mega city of China. Atmos. Environ. 44, 3187–3195.

Zhang, J., Zhou, X., Wang, Z., Yang, L., Wang, J., Wang, W., 2018. Trace elements in PM(2.5) in Shandong province: source identification and health risk assessment. Sci. Total Environ. 621, 558–577.

Zhang, J., Cheng, H., Wang, D., Zhu, Y., Yang, C., Shen, Y., et al., 2021. Chronic exposure to PM(2.5) nitrate, sulfate, and ammonium causes respiratory system impairments in mice. Environ Sci Technol 55, 3081–3090.

Zhou, M., Wang, H., Zeng, X., Yin, P., Zhu, J., Chen, W., et al., 2019. Mortality, morbidity, and risk factors in China and its provinces, 1990–2017: a systematic analysis for the Global Burden of Disease Study 2017. Lancet 394, 1145–1158.